©*Proc. Indian natn. Sci. Acad.*, 52, A, No. 1, 1986, pp. 67–101.
Printed in India

NUMEROUS STRUCTURES OF OXIDES CAN BE BUILT UP FROM THE ReO_3-TYPE FRAMEWORK*

B RAVEAU

Laboratoire de Cristallographie, Chimie et Physique des Solides, Equipe Oxydes, U.A. 251, ISMRa—Université de Caen, 14032 CAEN Cedex, France

Key Words : Oxide Structures; ReO_3-Type Framework; Aurivillius Phase; Perovskite

INTRODUCTION

THE perovskite structure, or more exactly the ReO_3-type lattice forming this structure is one of the most fascinating frameworks owing to its great simplicity and flexibility. Galasso,[1] Wells[2] and Rao *et al.*[3] have shown that the perovskite structure is involved in a great number of oxides. Moreover it appears, from the latter review that many structures are related to the perovskite. The aim of the present paper is to analyze the "MO_3" framework and to show that it can be used as a precursor for generation of new structural families, and also that some structures which are known since a long time are in fact closely related to the "MO_3" host-lattice.

THE ReO_3-TYPE HOST-LATTICE

The consideration of the ReO_3 structure (Fig. 1*a*) or of the cubic ABO_3 perovskites (Fig. 1*b*) shows that they are both formed of the same octahedral framework MO_3. This host lattice can be described as built up from "M_4O_{20}" units forming square tunnels (Fig. 2*a*) connected through the corners of their octahedra (Fig. 2*b*). The only difference between ReO_3 and the cubic perovskite concerns the occupancy of the tunnels which are empty in ReO_3 and fully occupied in the stoichiometric ABO_3 perovskites, while a partial and random occupancy is possible as shown in the bronzes A_xWO_3 for A = Li, Na, Ln, Ca, Sr, U, Cd, Hf (for review see ref. 4–6). A great number of stoichiometric perovskites exhibit a distorted MO_3 host-lattice which corresponds to a deformation of the MO_6 octahedra.[1] Another way of distorting the MO_3 framework corresponds to its compression or elongation along one [100] direction : it results in diamond-shaped "M_4O_{20}" units (Fig. 3) in which the MO_6 octahedra may remain regular. Many diamond shaped-tunnel perovskites[7–11] have been recently isolated involving Jahn-Teller ions such as Cu^{2+} and Mn^{3+}. It is for instance the case of the oxides $[CaCu_3]_AM_4O_{12}$ (M = Ti, Mn) and $[CaMn_3]_AMn_4O_{12}$ in which three A sites out of four are occupied by the Jahn Teller ions in an ordered way, and of the defect perovskites $(Cu\ \square)_ATa_2O_6$ and $(Mn\ \square)_AMn_4O_{12}$ in which vacancies and Jahn-Teller ions are distributed in an ordered way on the A sites. Those cubic perovskites whose "a" parameter is twice that of the ideal

*Presented at the INSA Golden Jubilee Symposium on Solid State Chemistry held at INSA, New Delhi during December 4–6, 1985.

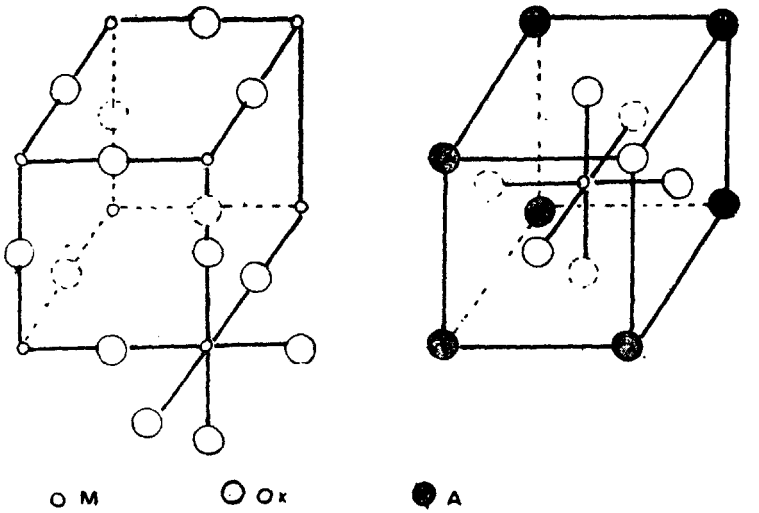

FIG 1 The usual representation of the ReO_3-structure (*a*) and of the perovskite structure AMO_3 (*b*).

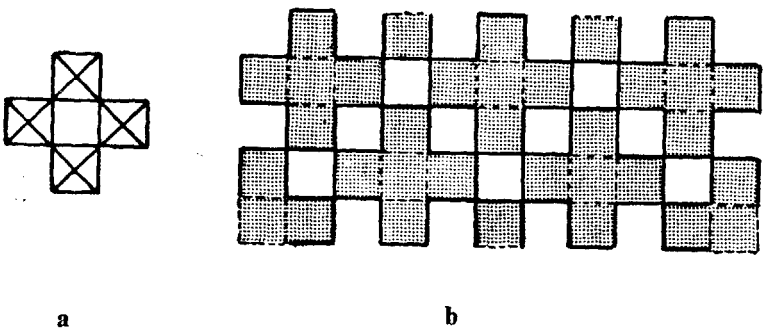

FIG 2 The octahedral "M_4O_{20}" units forming square tunnels (*a*) and their connection forming the MO_3 framework (*b*).

perovskite result from a compression of the ideal MO_3 framework and a tilting of the MO_6 octahedra (Fig. 4). This effect is a consequence of the presence of the Jahn-Teller ions Cu^{2+} or Mn^{3+} which take no more a 12-fold but a square planar coordination.

Thus it appears that the square "M_4O_{20}" units and the diamond shaped "M_4O_{20}" units are the two extreme units which can participate to the formation of the "MO_3" perovskite host-lattice. Consequently, one can imagine that the great ability of deformation of the perovskite "MO_3" framework without a sensible distortion of the MO_6 octahedra, should allow a great adaptability to various frameworks and polyhedra and to generate new structures closely related to perovskite.

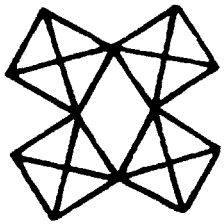

FIG 3 The diamond-shaped "M_4O_{20}" units.

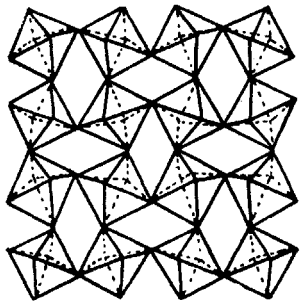

FIG 4 The diamond-shaped $CaCu_3M_4O_{12}$ perovskite.

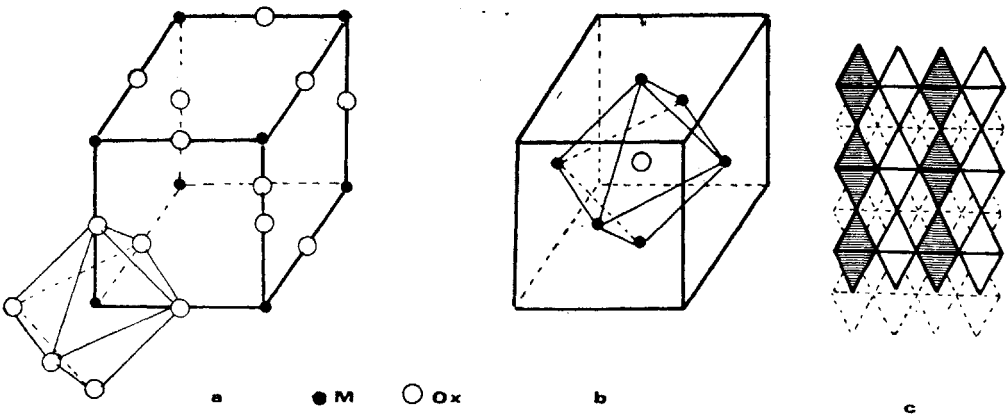

FIG 5 Description of the sodium chloride type structure of the MO oxides : (*a*) the $[MO_3]^{4-}$ ReO_3-type framework (*b*) the anti-ReO_3 $[OM_3]^{4+}$ framework and (*c*) interpenetration of the two octahedral frameworks.

THE ADAPTABILITY OF THE ReO_3-TYPE FRAMEWORK TO OTHER OCTAHEDRAL STRUCTURES

The ReO_3-Lattice and the Sodium Chloride Structure

A very well-known structure, which is often the first structure taught to the students is the one of sodium chloride owing to its cubic face centered character involving an *ABC* close-packing of the anions and of the cations. In fact, this structure is rather complexe and derives from the ReO_3-framework. The examination of the MO sodium chloride type oxides shows that a quarter of the metallic M atoms and three quarters of the oxygen atoms form a ReO_3-type lattice built up from corner-sharing MO_6 octahedra (Fig. 5*a*), whereas the remaining M and oxygen atoms form a OM_3 lattice built up of corner-sharing OM_6 octahedra (Fig. 5*b*) whose dimensions are identical to those of the MO_6 octahedra. Thus it appears that the MO-sodium chloride structure is composed of two interpenetrated and isometric $[MO_3]^{4-}$ and $[OM_3]^{4+}$ farmeworks (Fig. 5*c*) : the first one exhibits the ReO_3 structure whereas the second is an anti-ReO_3 framework.

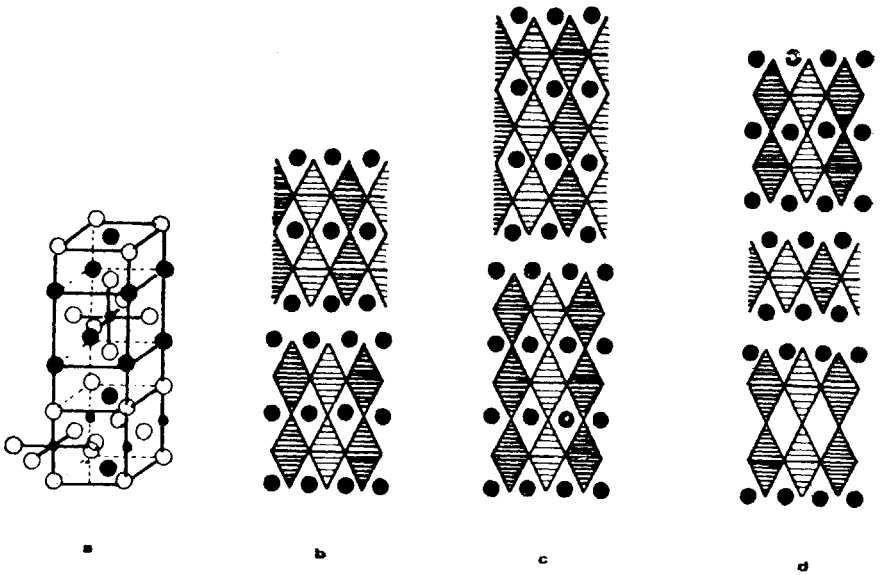

FIG 6 Structure of the intergrowths between perovskite and sodium chloride type oxides $(AO).(AMO_3)_n$: structure of the K_2NiF_4-type, $n = 1$ (*a*) and schematic representations of the members $n = 2$ (*b*), $n = 3$ (*c*) and $n = 1.5$ (*d*).

The close relationship of the perovskite structure with the sodium chloride structure is also clearly visible by considering the "*A*O" planes of the AMO_3 perovskite at the level $z = 0$ (Fig. 1*b*) which are characterized by sodium chloride type arrangement of the *A* and O ions. A consequence of this bidimensional accord between the *A*O rock salt structure and the AMO_3 perovskite leads to the generation of intergrowths $AO\ (AMO_3)_n$.[5,12–20] These phases consist of single sodium chloride type layers alternating with multiple perovskite layers, which are *n* octahedra thick (Fig. 6). Several series of oxides $AO\ (AMO_3)_n$ have been synthesized for A = Ca, Sr, Eu^{II} and M = Mn, Ti; many oxides exhibit the K_2NiF_4 structure which corresponds to the first number of the series : La_2CuO_4, La_2NiO_4, Sr_2MO_4 (M = Ti, Sn, Mn, Mo, Rn, Ir, Rh), Ba_2MO_4 (M = Sn, Pb), A_2UO_4 (A = K, Rb, Cs). The order between the *A*O and AMO_3 layers decreases as the thickness of the perovskite layers increases so that for very high n ($n \rightarrow \infty$) values the *A*O layers appear in the form of bidimensional defects in the perovskite matrix. Moreover, it must be pointed out that for non-integral *n* values multiple intergrowths corresponding to a sequence of several different perovskite layers (Fig. 6*d*) may be obtained; however, such intergrowths have never been observed in the ordered state.

The Diamond-shaped ReO_3-Framework and the Hexagonal Tungsten Bronze Structure (HTB)[21–32]

The comparison of the idealized diamond-shaped ReO_3 host-lattice (Fig. 7*a*) and of the H.T.B. A_xWO_3 (Fig. 7*b*) shows that these two structures are formed of

identical octahedral layers characterized by angles of 60 and 120°. The intergrowth of these structural types, can be realized by means of these layers (Fig. 7*c*). Thus, a series of bronzes A_xWO_3 (A = K, Rb, Tl, Cs, Sn, Pb, Sb) called intergrowth tungsten bronzes (ITB), and dielectric oxides $A_xM_xW_{1-x}O_3$ (A = K, Rb, Tl, Cs) called bronzoids were isolated. Fig. 7*c* shows as an example the structure of one of these ITB's observed for the bronzoids $Cs_x(Nb_xW_{1-x})O_3$. Several ordered ITB's in which the HTB and diamond-shaped perovskite slabs exhibit different thicknesses were isolated. Many disordered intergrowths were observed. Most of the ITB's are characterized by the presence of tungsten in the MO_3 framework, except for $Sb_{0.2}MoO_{3.1}$, $Ca_2TlTa_5O_{15}$ and the oxides $ACu_3M_7O_{21}$ (A = K, Rb, Tl, Cs and M = Nb, Ta).[30] The copper compounds are rather different from the other ITB's (Fig. 8) in that the Cu^{2+} ions which exhibit a square planar coordination are located in the diamond-shaped perovskite tunnels; the realisation of such a coordination for copper necessitates a tilting of the MO_6 octahedra along the c-direction perpendicular to the plane of the projection involving a doubling of the c-parameter with respect to the other ITB's. As a consequence this latter structure must be considered as modified ITB's, resulting from the intergrowth of the diamond shaped perovskite $Cu_3 \square M_4O_{12}$ and of the HTB's AM_3O_9. It is clear that such an intergrowth is initiated by the Jahn-Teller effect of copper.

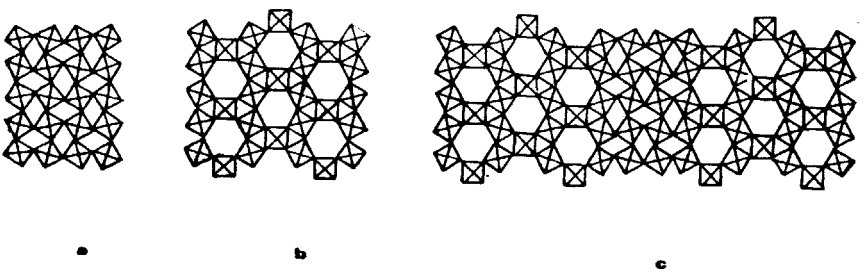

FIG 7 The idealized MO_3 host lattice (*a*) and the HTB framework (*b*) and the ITB $Cs_x(Nb_xW_{1-x})O_3$ (*c*).

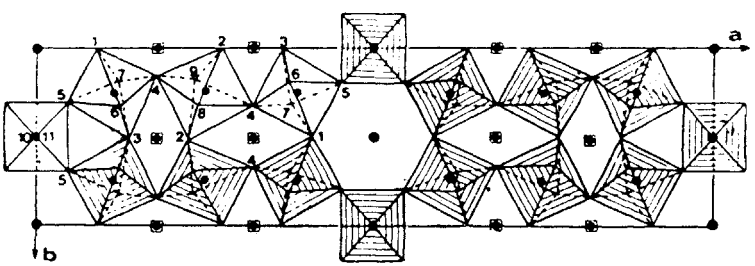

FIG 8 The modified ITB $ACu_3M_7O_{21}$, intergrowth of the diamond-shaped perovskite $Cu_3 \square M_4O_{12}$ and of the HTB AM_3O_9.

The M_4O_{20} Perovskite Columns and the TTB Structure[6,33–43]

The MO_3 perovskite framework is closely related to the tetragonal tungsten broze structure discovered by Magnéli. The rotation of a M_4O_{20} perovskite column in a ReO_3-type matrix (Fig. 9*a*) of $\pi/4$, leads to the formation of TTB microregions characterized by four pentagonal tunnels surrounding a square perovskite tunnel. Such an intergrowth is not so easy to realize, owing to the fact that it involves a small distortion of the MO_6 octahedra (Fig. 9*b*).

The presence of such isolated defects, in the form of TTB columns in the MO_3-perovskite matrix has been observed by high resolution electron microscopy WO_3–Nb_2O_5 system for the tungsten-rich compositions. It is obvious that the ordered formation of such "defects" in the ReO_3-type matrix should lead to a series of microphases. The limit phase is in fact represented by the TTB structure observed for $K_{0.50}WO_3$ (Fig. 9*b*) and $Nb_8W_9O_{47}$ (Fig. 9*c*) in which the "rotation defects" are so close to each other that no more place is left for the initial ReO_3-type matrix. Intermediate structures, which are intergrowths of the TTB and MO_3-perovskite structures can thus be predicted. The Nb_2O_5–WO_3 system is a good example in which the TTB–ReO_3-type intergrowths are easily formed. Fig. 10 shows, for example, the structure of $Nb_8W_{22}O_{86}$ and the formation of the TTB slabs in the ReO_3-type matrix by ordered rotation of the "M_4O_{20}" units. Such an inter-

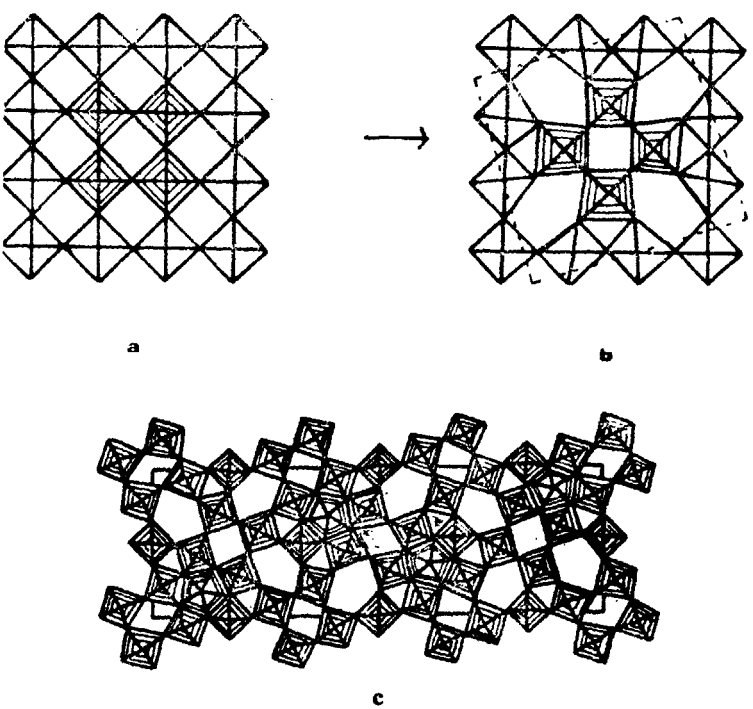

FIG 9 The rotation of a "M_4O_{20}" unit in a ReO_3-type matrix (*a*) leads to a TTB region (*b*) also observed for $Nb_8W_9O_{47}$ (*c*).

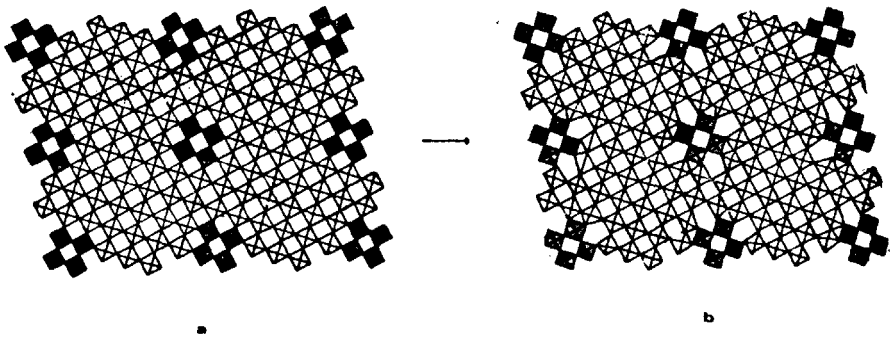

FIG 10 The cooperative rotation of the "M_4O_{20}" units (*a*) in a ReO_3-type matrix leading to the formation of the TTB slabs (*b*) in the ReO_3-type matrix.

growth can be formulated $[(MO)_2M_{10}O_{30}]^{TTB}$ $[MO_3]_{2n}^{ReO_3}$ with $n = 9$, where n corresponds to the number of octahedra forming the ReO_3-type chains between two TTB slabs and determines the width of the ReO_3-type slabs whereas $(MO)_2$ represents the number of "MO" chains located in the pentagonal tunnels of the TTB slabs. Thus a general formulation $[(MO)_xM_{10}O_{30}]_m^{TTB}$ $[MO_3]^{ReO_3}$, can be proposed for the different ordered intergrowths of this system where m and n are integral numbers corresponding to the width of the TTB and ReO_3-type slabs respectively and x is a non-integral number ($x < 4$) corresponding to the insertion rate of the MO chains in the pentagonal tunnels.

The oxides $Nb_8W_{22}O_{86}$ and $Nb_4W_7O_{31}$ correspond to the members $m = 1$ with $n = 9$ and 5 respectively, while $Nb_{12}W_{11}O_{63}$ is characterized by the values $m = 2$ and $n = 5$.

The TTB slabs are frequently disordered with variable widths, involving a wide domain of non-stoichiometry which is amplified by a variable insertion rate in the pentagonal tunnels. Analogous phenomena are observed in the Ta_2O_5–WO_3 system.

SHEAR STRUCTURE DERIVED FROM THE ReO_3-TYPE LATTICE[2–6,44–66]

The shear-structures derived from the ReO_3-type lattice over a wide field of investigation ranging from the molybdenum and tungsten suboxides M_nO_{3n-1} and M_nO_{3n-2} to the block structures derived from the M, N and H Nb_2O_5 forms. It is not possible to discuss here in a detailed way all those structures owing to their very great number : examples of a simple shear structure Mo_9O_{26} and of a block structure M-Nb_2O_5 are presented on Fig. 14*a* and 11*b* respectively. From their examination it is obvious that they are closely related to the MO_3 framework and derive from the latter by sharing the edges of their octahedra instead of their corners. It must simply be emphasized that the true single shear structures are formed of ReO_3-type slabs separated by infinite crystallographic shear planes (CSP) in which the MO_6

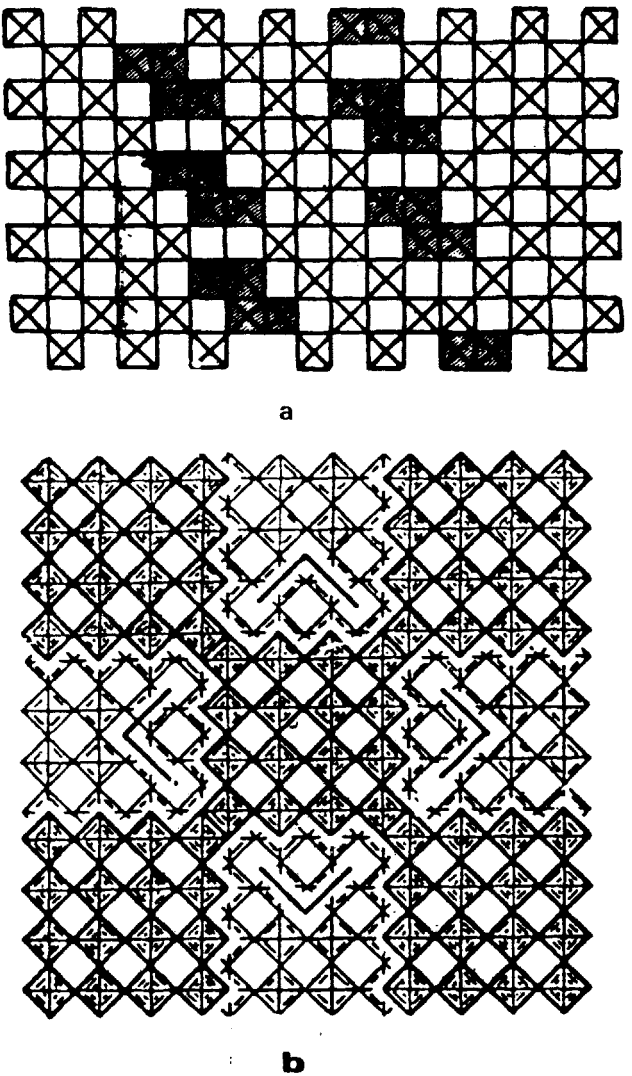

FIG 11 Structures of a true single shear structure Mo_9O_{26} (*a*) and of a block-structure *M*-Nb_2O_5.

octahedra share their edges, whereas the block structures result from a combination of several shearing phenomena leading no more to perovskite slabs but to MO_3^- perovskite columns sharing the edges of their octahedra.

It is well known that the direction of the CSP's in those structure depends on the number of octahedra sharing their edges. The most frequent CSP's {102} {103} and {001} or {100} are formed of blocks of 2×2, 2×3 and $2 \times \infty$ edge-sharing octahedra respectively (Fig. 12). It must be pointed out that these CSP's formed of $2 \times n$ edge-sharing octahedra, are themselves built up from edge-sharing "M_4O_{20}" units for even-*n* values (Fig. 12 *b* and *e*).

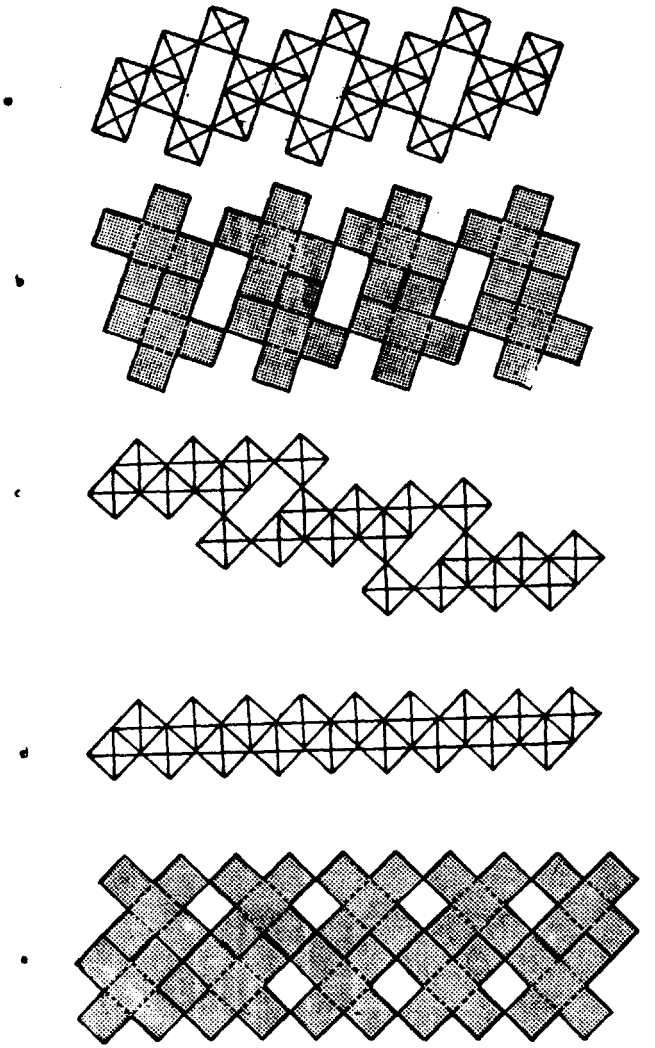

FIG 12 The most current crystallographic shear planes {102} (*a*, *b*), {103} (*c*), {001} (*d*-*e*).

Besides the {102} and {103} C.S.P. which lead to the formation of the M_nO_{3n-1} and M_nO_{3n-2} shear structures respectively, the {001} C.S.P. exhibits a particular interest in that they can be formed in two different ways noted $\{001\}^a$ (Fig. 13*a*) and $\{001\}^b$ (Fig. 13*b*), leading always to oxides of formulation M_nO_{3n-1}. It results that two other different series of M_nO_{3n-1} can be considered : the oxides characterized by the presence of one type of CSP's only (*a* or *b* considered separately are equivalent), and the oxides in which the two types of CSP $\{001\}^a$ and $\{001\}^b$ coexist in the structure. An example of the first series is given by Nb_3O_7F or V_2MoO_8 third member of the series (Fig. 13*c*) whereas an example of the second series is given by P-Nb_2O_5 (Fig. 13*d*) second number of the series. It is remarkable that first number of this second series (Fig. 13*e*) corresponds to a very compact structure

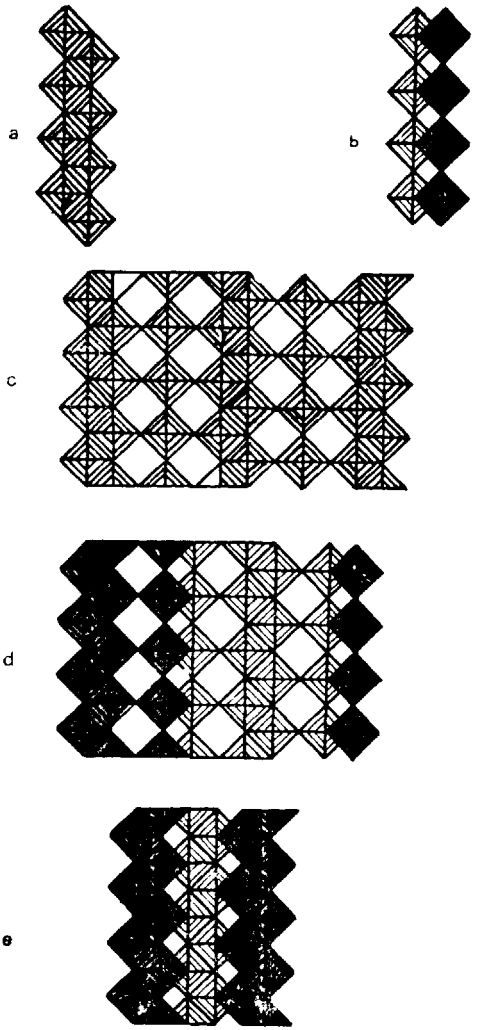

FIG 13 The M_nO_{3n-1} shear structures. The two representations of {001} CSP's (*a*) and (*b*); comparison of the structure of the oxides V_2MoO_8 (*c*), P—Nb_2O_5 (*d*) and idealized anatase TiO_2 (*e*).

only built up from edge-sharing octahedra; this latter structure is in fact observed for the anatase form of TiO_2 with a sensible distortion of the octahedra. Consequently these C.S. structures can be considered as a result of the adaptability of the ReO_3-type framework to the MO_2-anatase structure.

LAYER STRUCTURES

The great flexibility of the ReO_3-type framework makes that the perovskite structure can also be "cut up" in the form of anionic layers whose cohesion is ensured either

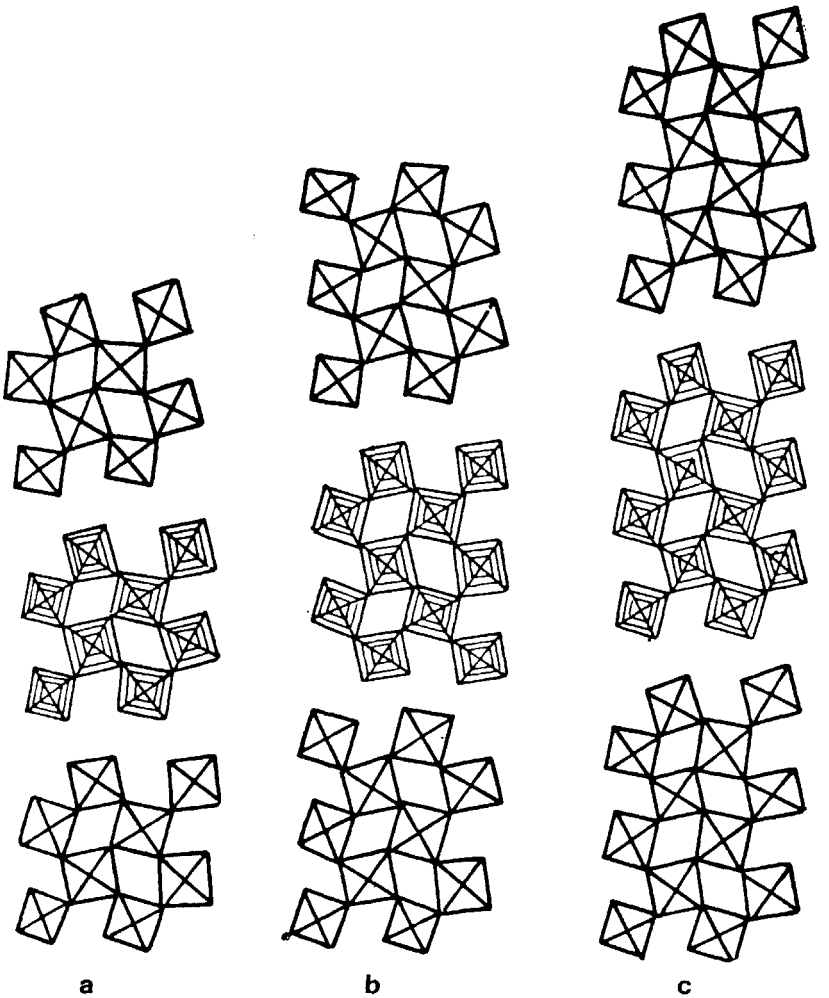

FIG 14 The layer titanates and titanoniobates $A_nM_nO_{3n+2}$: $n = 4$ (*a*), $n = 5$ (*b*) and $n = 6$ (*c*).

by A^{2+} ions like in the layer oxides $A_nM_nO_{3n+2}$ or by infinite cationic layers $[Bi_2O_2]_n^{2n+}$ like in the Aurivillius phases.

The Titanates and Titanoniobates $A_nM_nO_{3n+2}$ with a Layer Structure[63–67]

These compounds form a very important family in which A is an alkaline-earth ion and or a lanthanide ion and M is titanium and or niobium. The different members of the series were isolated in the systems $A_2Nb_2O_7$–$CaTiO_3$ (A = Ca, Sr) and $Ln_2Ti_2O_7$–$CaTiO_3$ (Ln = La, Nd). Their structure consists of infinite anionic layers $[M_nO_{3n+2}]^{n'-}$ ($2n \leqslant n' \leqslant 3n$), whose cohesion is ensured by A^{2+} and A^{3+} cations. These layers exhibit a diamond-shaped perovskite configuration, with distorted MO_6 octahedra. The different members of the series (Fig. 14) differ from

each other by the number n of octahedra which determines the thickness of the perovskite layers, the smallest member which has been observed in oxides being $Ca_2Nb_2O_7$ ($n = 4$). Non integral n values are also observed : they correspond to the stacking of layers of different thickness in the same oxide; these latter oxides are considered as intergrowths of two or several integral-n members. Such intergrowths may be ordered, or disordered, formed of two or more different n-members leading to giant cells which have been observed by electron microscopy.

The Aurivillius phases $Bi_2O_2A_{n-1}M_nO_{3n+1}$[2–3,5,68–77]

The Aurivillius phases, which have been extensively studied for their ferroelectric properties form a very numerous family which can be formulated $(Bi_2O_2)^{2+}$ $(A_{n-1}M_nO_{3n+1})^{2-}$ with A = Ca, Sr, Ba, Pb, K, Na, Bi and M = Ta, Nb, Ti, W.

This structural family is represented on Fig. 15 by the three first members, the koechlinite Bi_2MoO_6 ($n = 1$) studied for its catalytic properties and the ferroelectric oxides $Bi_2SrNb_2O_9$ ($n = 2$) and $Bi_4Ti_3O_{12}$ ($n = 3$).

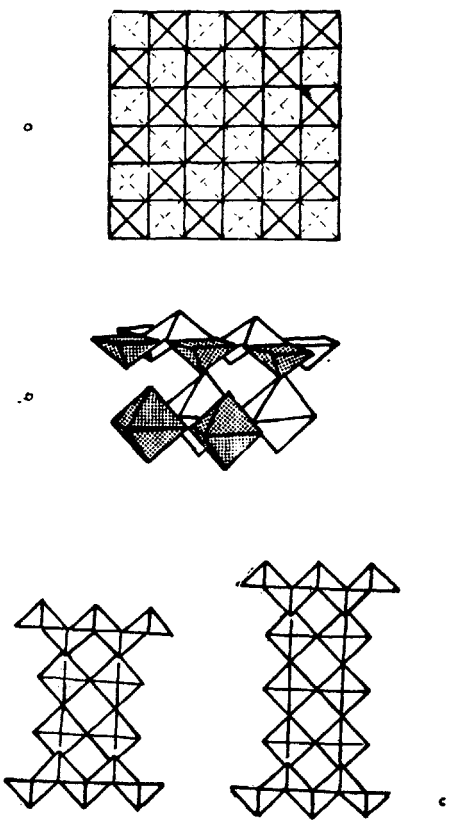

FIG 15 The Aurivillius phases. The $(Bi_2O_2)^{2+}$ layer (*a*) koechlinite, $n = 1$ (*b*) schematic representation of $Bi_2SrNb_2O_9$ $n = 2$ (*c*) and $Bi_4Ti_3O_{12}$, $n = 3$ (*d*).

The structure of the different integral m members is formed of pyramidal $(Bi_2O_2)^{2+}$ layers (Fig. 15*a*) built up of edge-sharing BiO_4 pyramids alternately with multiple perovskite layers (Fig. 15*b*, *c*, *d*) which are n octahedra thick. This class of oxides is very similar to the $(AO).(AMO_3)_n$ intergrowths : the $(Bi_2O_2)^{2+}$ layers replace the sodium-chloride AO slabs whereas the perovskite slabs remain untouched. Nevertheless the $AO(AMO_3)_n$ oxides form a continuous three dimensional material and cannot be considered as a layer-structure contrary to the Aurivillius phases which consist of cationic and anionic infinite layers. The non-stoichiometry possibilities in these oxides are similar to those described for (AO) $(AMO_3)_n$, as well as for $A_nM_nO_{3n+2}$: for non integral n values and high n values ordered and disordered intergrowths of integral members are observed.

The structure of MoO_3[78]

The structure of MoO_3 formed of neutral layers of edge-sharing distorted octahedra, whose cohesion is ensured by van der Waals forces can be deduced from the ReO_3-type framework in a very simple way, as shown formally on Fig. 16. The cooperative migration of one plane of MoO chains out of two in the MO_3-perovskite framework, i.e. the 001 shearing of one octahedral layer out of two (Fig. 16*a*) leads to double edge sharing MO_3-perovskite layers already observed in {001} M_nO_{3n-1} shear structures (Fig. 16*b*). The translation of one layer out of two along the direction perpendicular to the plane of the projection of half a height of an octahedron combined with a simple translation in this plane in order to bring them closer together leads to the MoO_3 layer structure (Fig. 16*c*). Thus, it appears that the MoO_3 structure can be considered as the consequence of a shearing mechanism in the ReO_3-type lattice.

Adaptability of the ReO_3-type Framework and Tetrahedra

The ability of the ReO_3-type framework to adapt PO_4 tetrahedra has been discovered recently with the very numerous family of the phosphate tungsten bronzes.[79–90] These oxides are generated by the replacement of one or two octahedra by a PO_4 tetrahedron or a diphosphate group in a "W_4O_{20}" unit (Fig. 17). The O–O distance in the PO_4 tetrahedra, very close to those observed in the WO_6 octahedra, allows a junction without changing the angles of 90° which characterize the perovskite cagss (Fig. 17*a*). In the same way the height of the P_2O_7 group, close to that of a WO_6 octahedron, allows a connection without tilting drastically or distordering the WO_6 octahedra (Fig. 17*b*). As a result four main families of phosphate tungsten bronzes closely related to the perovskite have been isolated : the diphosphate tungsten bronzes with hexagonal tunnels ($DPTB_H$), the monophosphate bronzes with pentagonal tunnels ($MPTB_P$), and the diphosphate tungsten bronzes with pentagonal tunnels ($DPTB_P$), all characterized by metallic or semi-conductive properties.

The $DPTB_H$'s $A_x(P_2O_4)_2(WO_3)_{2m}$ (A = K, Rb, Tl, Ba; $0 < x \leqslant 1$ and m = integral) have their host-lattice $(P_2O_4)_2(WO_3)_{2m}$ formed of ReO_3-type slabs connected through planes of diphosphate groups (Fig. 18). The "perovskite" slabs are almost regular and their perovskite tunnels are empty. At the junction between two

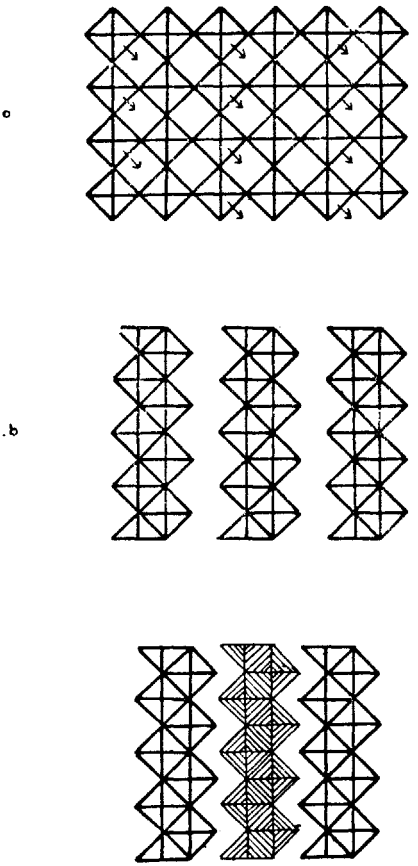

FIG 16 Cooperative migration of the MO chains in the ReO_3-type structure (a) leading to {001} CSP's (b) and finally to the MoO_3 structure.

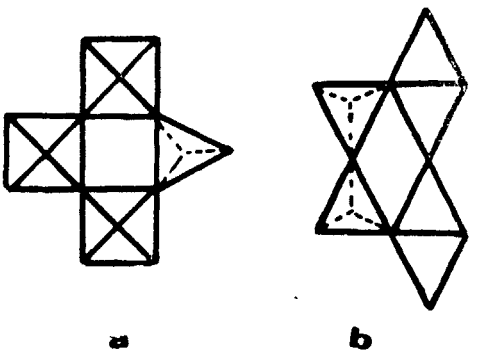

FIG 17 The adaptability of a tetrahedron (a) and of a P_2O_7 group (b) to the WO_6 octahedra.

consecutive slabs the corner-sharing WO_6 octahedra and P_2O_7 groups form hexagonal tunnels where the A ions are located. The ReO_3-type slabs have a variable

width characterized by the number m of corner sharing octahedra in the $[100]_P$ direction. Moreover, the even-m members (Fig. 18*a*) differ from the odd-m members (Fig. 18*b*) by a translation of one phosphate plane out of two. As a consquence, the perovskite slabs are all built up of identical chains of $m/2$ octahedra in the $[010]_P$ direction of the even-m members (Fig. 18*a*), whereas in the odd-m members, the octahedra chains parallel to $[010]_P$ of one slab are alternately formed of $\frac{m+1}{2}$ and $\frac{m-1}{2}$ octahedra (Fig. 18*b*). The tendancy to form regular tunnels is remarkable : the hexagonal tunnels exhibit angles of 90 and 120°, while the perovskite tunnels are characterized by angles very close to 90°, and 60–120° are observed for the small diamond-shaped tunnels built up from two octahedra associated to two tetrahedra.

The $MPTB_P$'s $(PO_2)_4(WO_3)_{2m}$ are also built up from ReO_3-type slabs connected through phosphate planes (Fig. 19) but in these oxides each PO_4 tetrahedron shares its four corners with WO_6 octahedra. At the junction between two perovskite slabs the WO_6 octahedra and PO_4 tetrahedra form pentagonal tunnels which are empty. Like the $DPTB_H$'s, the different members of this series differ from each other by the width of the ReO_3-type slabs i.e. by the number m of octahedra in the $[001]_P$ direction and by the parity of m. In the even-m members (Fig. 19*a*) the perovskite slabs exhibit a constant width along $[110]_P$, whereas in the odd-m members (Fig. 19*b*) one phosphate plane out of two has been translated so that chains $\frac{m+1}{2}$ and $\frac{m-1}{2}$ octahedra alternate parallel to the $[110]_P$ direction. Moreover, in this series, the member $m = 5$, exhibits a second form whose host-lattice (Fig. 19*c*) is formed

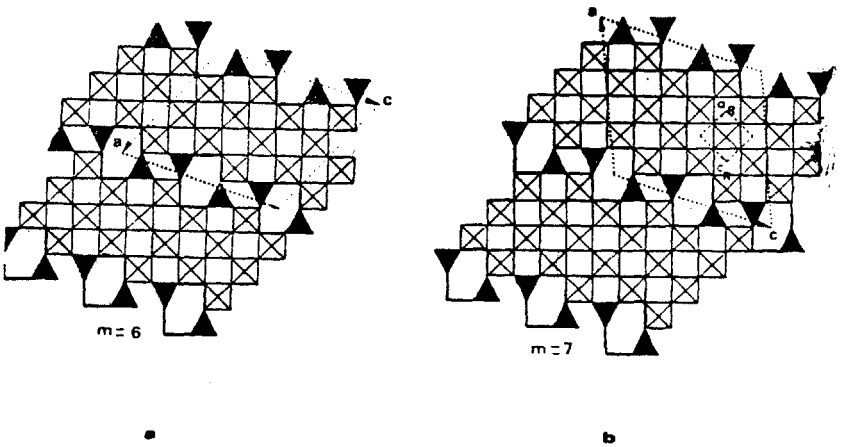

a b

FIG 18 The structure of $DPTB_H$'s $(P_2O_4)_2(WO_3)_{2m}$. (*a*) an even-m member $m = 6$ (*b*) an odd-m member $m = 7$.

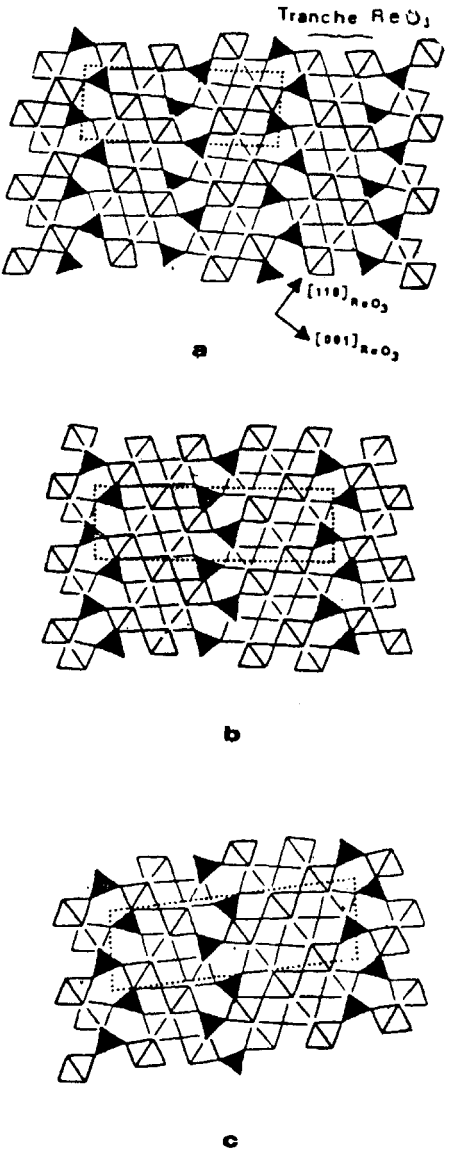

FIG 19 Structure of the $MPTB_P$'s $(PO_2)(WO_3)_{2m}$ an even m member $m = 4$ (*a*); an odd-m member $m = 5$ (*b*); the second form of observed for $m = 5$ corresponding to the intergrowth of $m = 4$ and $m = 6$ (*c*).

of two different ReO_3-type slabs which are six and four octahedra wide respectively, so that such a structure can be considered as an intergrowth of the two even members, $m = 4$ and $m = 6$.

The third family, the $MPTB_H$'s $A_x(PO_2)_4(WO_3)_{2m}$, is observed for $A =$ Na, K and an insertion rate greater than that of the $DPTB_H$'s $1 < x \lesssim 2$. The structure

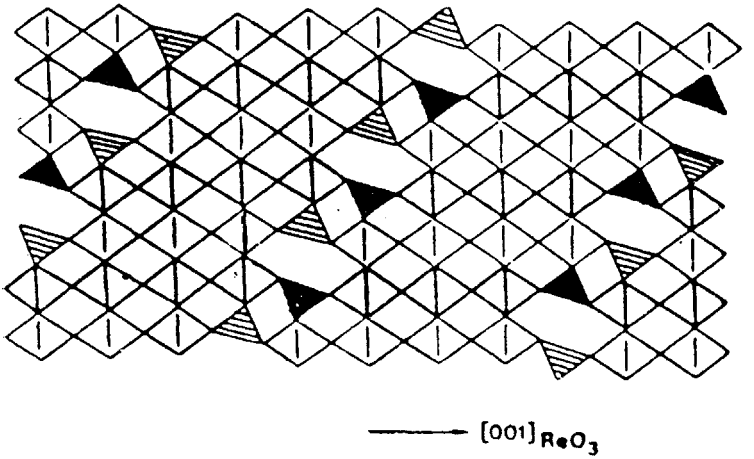

a

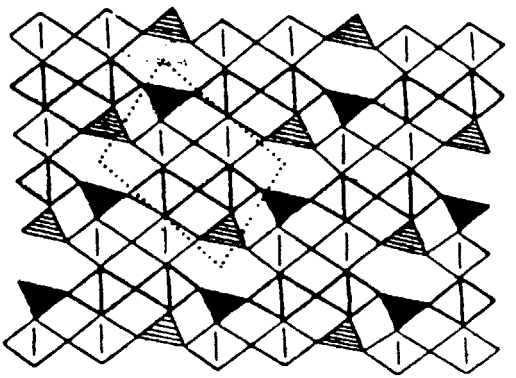

b

FIG 20 Structure of the $MPTB_H$'s $K_x(PO_2)_4(WO_3)_{2m}$ an odd-m member $m = 7$ (a) an even-m member $m = 4$.

of these bronzes is composed of ReO_3-type slabs identical to those of the $MPTB_P$'s and connected through "monophosphate planes" (Fig. 20). These differ from the $MPTB_P$'s by their junction between two ReO_3-type slabs in which the PO_4 tetrahedra and WO_6 octahedra form hexagonal tunnels where the A ions are located. In these oxides the odd-m members (Fig. 20a) difler from the even-m members (Fig. 20b) by a translation of one phosphate plane out of two as shown for the potassium bronze $m = 4$ (Fig. 20b). It is worthy of note that both frameworks $MPTB_P$'s and $MPTB_H$'s are very closely related : they are both built up of quite identical MO_3 slabs

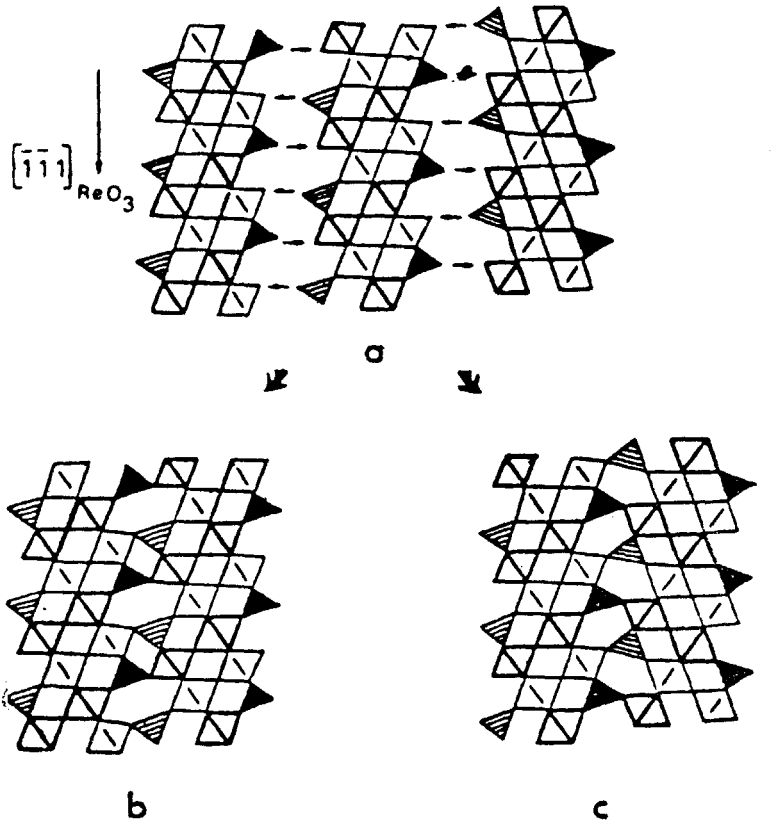

FIG 21 The identical MO_3-slabs bordered with PO_4 tetrahedra (*a*) common to the $MPTB_H$'s (*b*) and to the $MPTB_P$'s (*c*).

bordered by PO_4 tetrahedra (Fig. 21*a*) and differ only one from each other by the relative positions of the slabs. One passes from the $MPTB_H$'s structure (Fig. 21*b*) to the $MPTB_P$'s structure (Fig. 21*c*) by rotation of 180° of one slab out of two.

Besides these three classes of oxides which were synthesized in quantitative manner for a wide field of composition (*m* ranging from 4 to 16), the $DPTB_P$'s could be observed by HREM on microcrystals but could not be synthesized as pure compounds in the form of polycrystalline samples. The host-lattice of these bronzes (Fig. 22) is closely related to the one of $DPTB_H$'s in that one observes again MO_3-perovskite slabs connected through diphosphate planes. But, contrary to the $DPTB_H$'s, the association of two P_2O_7 groups and two WO_6 octahedra at the junction of two perovskite slabs delimits pentagonal tunnels which seem to be unoccupied. Moreover, only a semiregular spacing of the diphosphate planes could be observed for those oxides.

It must be pointed out that all these bronzes exhibit single and multiple intergrowths for non-integral *m*-values, and for very high integral *m*-values.

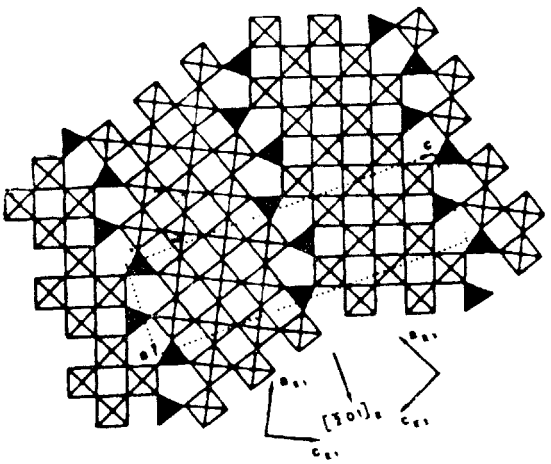

FIG 22 Idealized structure of the $DPTB_P$'s : the member $m = 7$ $(P_2O_4)(WO_3)_{2m}$.

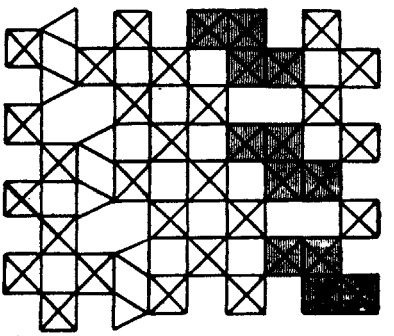

FIG 23 Transversal intergrowth of {102} CSP's and diphosphates planes.

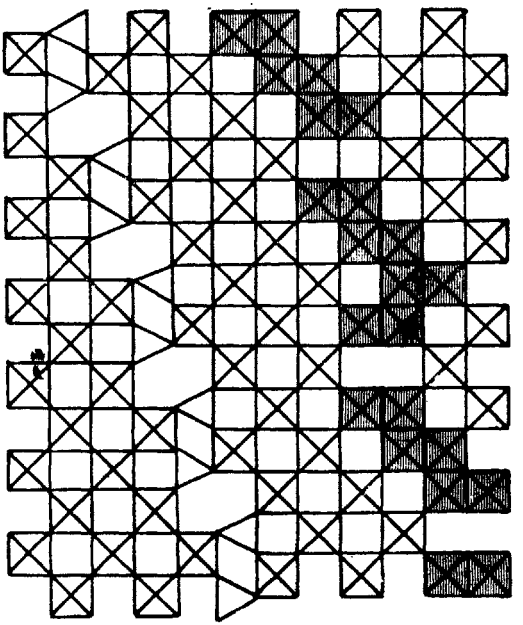

FIG 24 Transversal intergrowth of {001}—{103} CSP's and diphosphates planes.

These intergrowths which correspond to a sequence of different ReO_3-type slabs may be either ordered or disordered according to the method of synthesis and the nominal composition of the samples. Many extended defects have been observed in these oxides by HREM which show the great flexibility of the perovskite framework.

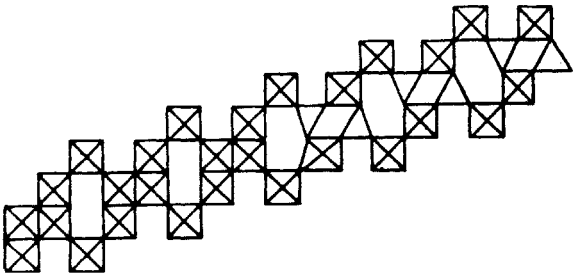

FIG 25 Longitudinal intergrowth of {102} CSP's and diphosphates planes.

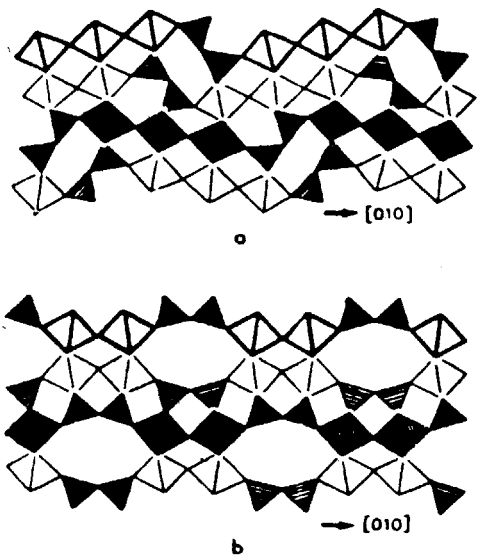

FIG 26 Structure of $P_8W_{12}O_{52}$ (*a*) and $CsP_8W_8O_{10}$ (*b*).

It is not possible to present here all these studies. Nevertheless one can mention as examples the possibility of formation of regular transversal inergrowths of {102} CSP and diphosphates planes in a MO_3 matrix (Fig. 23), or transversal intergrowths of complex {001}—{103} CSP and diphosphate planes (Fig. 24) or longitudinal intergrowths of {102} CSP and diphosphate planes (Fig. 25).

Besides these bidimensional conductors, other phosphorus tungsten oxides such as $P_8W_{12}O_{52}$[91] and $CsP_8W_8O_{40}$[92] emphasize the great adaptability of the PO_4 tetrahedra to the MO_3-perovskite framework. The first one has its framework (Fig. 26*a*) formed of perovskite columns built up of 2 × 3 octahedra which are linked together sometimes through the vertices of their octahedra, sometimes through diphosphate groups; this framework forms pentagonal, "hexagonal" and perovskite tunnels which are empty. The bronze $CsP_8W_8O_{40}$ whose host lattice (Fig. 26*b*) is formed of corner-sharing WO_6 octahedra and diphosphate groups is remarkable

by its octagonal tunnels where the Cs^+ ions are located. In spite of this particularity this structure is very closely related to the perovskite in that one observes "M_4O_{20}" units which form perovskite columns perpendicular to the plane of the projection. These columns are completely isolated, i.e. they are only linked to P_2O_7 groups so that such a bronze should present a unidimensional conductivity.

The possibility to adapt tetrahedra to the MO_3-perovskite lattice is not limited to the phosphate tungsten bronzes. The oxides γ and η Mo_4O_{11}[93–94] correspond to the members $m = 6$ of the $MPTB_P$'s and the $MPTB_H$'s respectively, while $NbPO_5$ and $NbTaO_5$[95] represent the second member of the $MPTB_P$'s. In the same way the molybdenum bronzes $A_xMo_6O_{17}$ (A = Na, K, $0.8 < x \leqslant 1$) which exhibit a layer structure[96–98] are related to the $MPTB_P$'s. Their structure (Fig. 27) is characterized by four octahedra-wide perovskite layers bordered by MO_4 tetrahedra; the cohesion between these layers is ensured by the A^+ ions.

Creation of Anionic Vacancies in the Perovskite Structure

The ReO_3-framework, owing to its great flexibility, is at the origin of new structural families, which can be deduced from the perovskite structure by ordered formation of anionic vacancies. In order to form AMO_{3-x} perovskites, the M cation must be able to take besides the octahedral coordination smaller coordinations (tetrahedral, pyramidal, square planar, etc...). Such a situation can be realized by the presence on the M sites either of two different metallic elements or of mixed valence elements. In this respect elements such as iron, copper, manganese and cobalt are potential candidates owing to their ability to take several oxidation states and several coordinations.

From Perovskite to β-*Cristoballite* via *Brownmillerite : Oxygen-Defect Perovskites built up from Octahedra and Tetrahedra*[99–114]

Starting from the ReO_3-type framework (Fig. 28*a*), new mixed frameworks can be generated by creation of rows of oxygen vacancies parallel to $[110]_P$ in an octa-

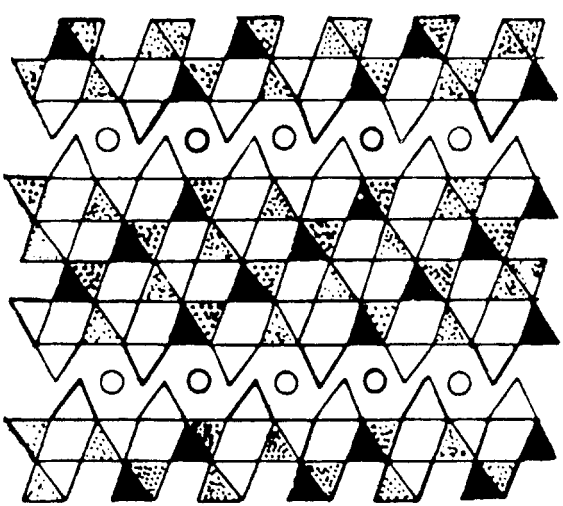

FIG 27 The structure of the molybdenum bronze AMo_6O_{17} (A = Na, K).

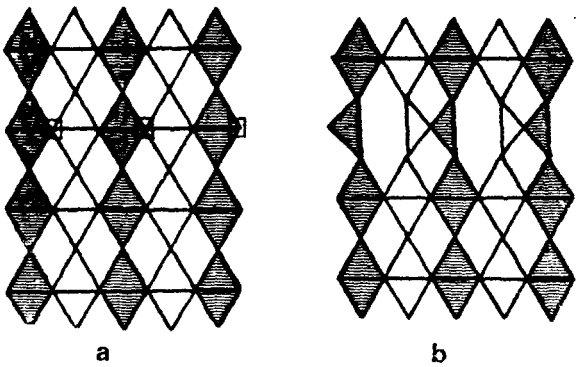

FIG 28 The creation of rows of oxygen vacancies in the MO_3 framework along $< 110 >_P$ (*a*) leads to the formation of slabs of tetrahedra (*b*).

hedral slab in such away that one vacant row alternates with a fully occupied one leading to a tetrahedral slab (Fig. 28*b*). This "mechanism" of formation of vacancies leads to the oxygen-deficient perovskites $(AMO_3)_nAMO_2\,\square$ whose host lattice is built up from multiple perovskite layers connected through planes of MO_4 tetrahedra as shown for the three first members of the series (Fig. 29). The integral number n corresponds to the number of octahedra which determines the thickness of the perovskite slabs. Numerous phases corresponding to different n values have been isolated in the systems $Ca_2Fe_2O_5$—$ATiO_3$ (A = Ba, Sr, Ca) and $Ca_2Fe_2O_5$—$AFeO_3$ (A = Y, La, Gd), in which iron exhibits simultaneously two coordinations, tetrahedral and octahedral, and one oxidation state + 3, and in the system $SrFeO_3$—$Sr_2Fe_2O_5$, where iron exhibits a mixed valence Fe^{3+}—Fe^{4+}. In all these oxides many intergrowths of two integral n-members have been observed for non integral m values as shown for instance for $Ca_5Fe_5O_{13}$ ($n = 1.5$) which corresponds to the intergrowth of the members m = 1 and 2 (Fig. 29*d*). More complexe ordered and disordered intergrowths are frequently observed in these systems in which iron can be partially replaced by manganese.

The brownmillerite structure $Ca_2Fe_2O_5$, also observed for Ca_2FeAlO_5, Ca_2FeCoO_5 and $Sr_2Co_2O_5$, first member of this series (Fig. 29*a*) differs from the other members of the series in that one layer of tetrahedra out of two is translated; it results a doubling of the b parameter with respect to the hypothetical structure (Fig. 30*a*) which would correspond to the same composition. If one carries on the process of ordered creation of rows of anionic vacancies parallel to $[110]_P$ in this latter structure (Fig. 30*a*), a tetrahedral framework is obtained (Fig. 30*b*) which is in fact the one of β-cristoballite.

Oxygen-Defect Perovskites and Related Structures built up from MO_6 Octahedra and MO_5 Pyramids[115–125]

The creation of rows of oxygen vacancies parallel to the [001] direction of the cubic perovskite cell leads to the formation of a series of oxides whose framework is built up of MO_5 pyramids and MO_6 octahedra. The resulting framework forms

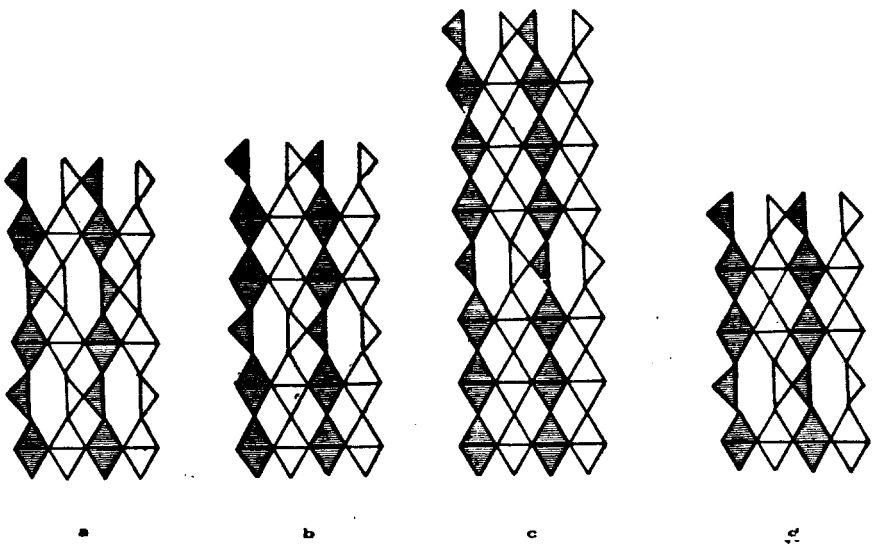

FIG 29 The oxygen defect perovskites $(AMO_3)_nAMO_2\square$ (*a*)—Brownmillerite $n = 1$, (*b*) $n = 2$, (*c*) $n = 3$, (*d*) $n = 1.5$ intergrowth of $n = 1$ and $n = 2$.

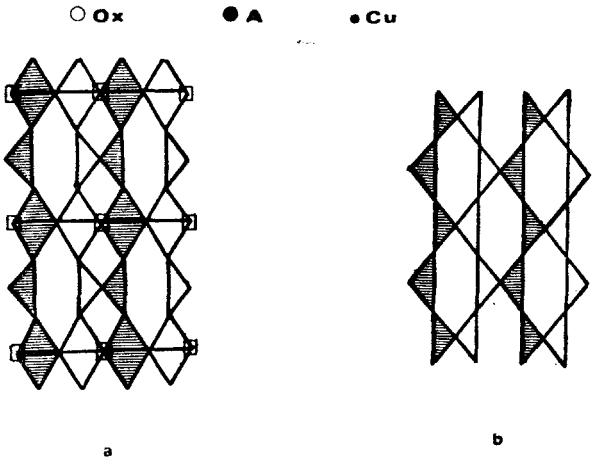

FIG. 30 Ordered creation of anionic vacancies in the hypothetical second form of $A_2M_2O_5$ first member of the series $(AMO_3)_nAMO_2\square$ leading to the β-cristoballite ($n = 0$) (*b*)

hexagonal tunnels where the *A* ions are located. Copper, cobalt and especially manganese oxides are characterized by their ability to form such oxygen defect perovskites. For instance the anion deficient system $CaMnO_{3-x}$ exhibits at least twelve different ordered oxygen-deficient perovskite structures : four different forms for the limit composition $CaMnO_{2.5}$, and four forms for $CaMnO_{2.75}$, two forms for $CaMnO_{2.667}$, and one form for $CaMnO_{2.556}$ and $CaMnO_{2.8}$. $Sr_2Mn_2O_5$, $Ca_2Co_2O_5$ and $BaLa_4Cu_5O_{13}$ belong to this class of compounds.

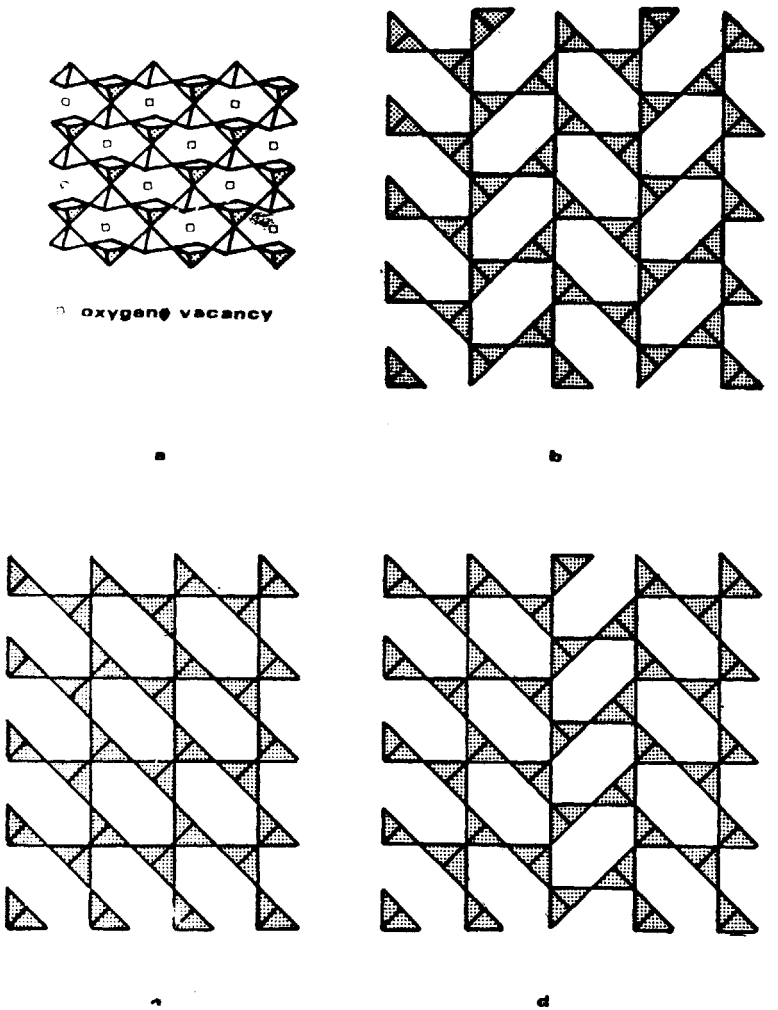

FIG 31 Structure of $Ca_2Mn_2O_5$—schematic drawings corresponding to the major form (*a* & *b*) showing the rows of oxygen vacancies parallel to $[001]_P$ in the ReO_3-type framework (*a*) and the MnO_5 pyramids forming rows of hexagonal tunnels (*b*) and schematic structures of two other minor forms (*c-d*) showing different orientations of the rows of tunnels.

A complete discussion of all these oxygen deficient perovskites is not possible here. Nevertheless it can be stated that all these frameworks result from the ordered elimination of rows of oxygen atoms parallel to $[001]_P$ in the ReO-type framework. The different forms of $Ca_2Mn_2O_5$ are all characterized by corner-sharing MnO_5 pyramids in agreement with the unique presence of the Jahn-Teller ion Mn(III); these forms differ only from each other by the relative orientation of the rows of hexagonal tunnels. It is easy to understand from the comparison of the structure of the most currently observed phase (Fig. 31*a*, *b*) for $Ca_2Mn_2O_5$ with

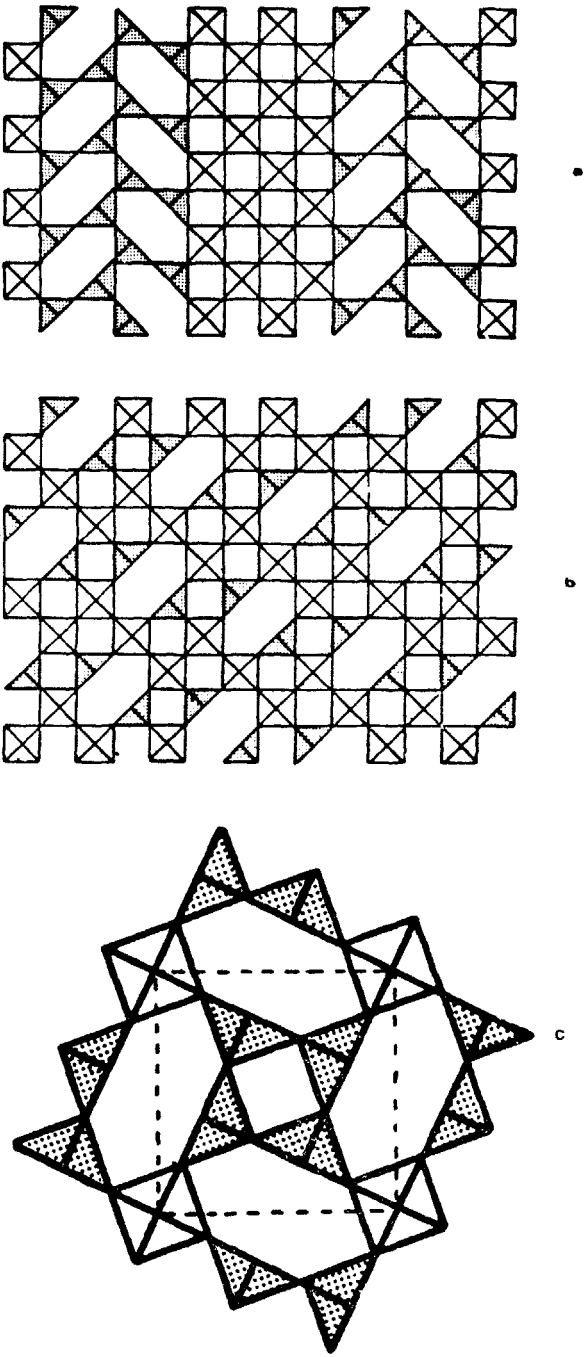

FIG 32 Some examples of ordered oxygen defect perovskites built up from corner-sharing MO_5 pyramids and MO_6 octahedra (*a*)—one form of $CaMnO_{2.75}$ (*b*) $Ca_2MnO_{2.80}$ (*c*) $BaLa_4Cu_5O_{13}$.

two other forms (Fig. 31*c*, *d*), observed in minor amounts, that many polytypes can be predicted; these phases consist of identical rows of hexagonal tunnels parallel to $[110]_P$ and differ from each other only by the relative orientation of the successive tunnel rows. The ordered insertion of oxygen in the hexagonal tunnels of the different $Ca_2Mn_2O_5$ forms may lead to mixed valence oxygen dificient perovskites built up from multiple rows of hexagonal tunnels, i.e. multiple slabs of MnO_5 pyramids parallel to $(110)_P$ which alternate with multiple ReO_3-type slabs as shown for instance for one form of $CaMnO_{2.75}$ (Fig. 32*a*) which is obtained by insertion of oxygen in the $Ca_2Mn_2O_5$ form described in Fig. 30*b*. Many other complex organisations of these hexagonal tunnels, resulting from mixed frameworks built up form octahedra and tetrahedra have been observed for intermediate compositions between $A_2M_2O_5$ and the stoichiometric perovskite as shown for instance for $Ca_2MnO_{2.8}$ (Fig. 32*b*) and the metallic conductor $BaLa_4Cu_5O_{13}$ (Fig. 32*c*).

The possibility of formation of mixed layers built up from MO_5 pyramids and MO_6 octahedra can be extended to the intergrowths $AO(AMO_3)_n$. The oxides $La_{2-x}A_{1+x}CuO_{6-x/2+\delta}$ (A = Ca, Sr) are one example of such a possibility : the structure of the limit compound $La_2SrCu_2O_6$ (Fig. 33*a*) corresponds to the second member of the intergrowth in which the AO layer remains stoichiometric whereas the double perovskite layer is oxygen-deficient in such away that it is only formed of corner-sharing CuO_5 pyramides. It is worthy of note that such a Cu(II)-oxide can intercalate oxygen in a reversible manner, leading to the mixed-valence oxides $La_2SrCu_2O_{6+\delta}$ in which the oxygen-deficient perovskite slabs are built up from CuO_6 octahedra and CuO_5 pyramids. The oxides $La_{2-x}A_xCu_{4-x/2+\delta}$ (A = Cu, Sr) are closely related to the oxides $La_{2-x}A_{1+x}Cu_2O_{6-x/2+\delta}$: they represent the first member of the intergrowth (Fig. 33*b*) formed of AO stoichiometric layers and single oxygen deficient perovskite layers. Moreover they differ from the second member, in that the oxygen vacancies are located in the basal plane of the CuO_6 octahedra. The mixed valence character of copper in these oxides, and their ability to intercalate oxygen make that they exhibit a *p*-type conductivity ranging from a semi-conductive to a metallic character.

Oxygen-Defect Perovskites and Related Structures involving Copper in Square Planar Coordination[126–132]

The ability of copper to take two oxidation states Cu II-Cu III and several coordinations—octahedral, pyramidal, square planar—makes that mixed valence oxygen-deficient perovskites or related structures can be isolated for copper oxides, in which copper exhibits the square planar coordination, The oxygen defect perovskite $La_3Ba_3Cu_6O_{14+\delta}$ and the isostructural oxides $Ba_3La_{3-x}Ln_xCu_6O_{14+\delta}$ (Ln = Pr, Nd, Sm, Eu, Gd, Yb, Er, Y), and the oxides $ACuO_2$ (A = Ca, Sr), A_2CuO_3 and $CaCu_2O_3$ derived from the perovskite are the main examples of this particular behaviour of copper.

The structure of the reduced from $La_3Ba_3Cu_6O_{14}$ (Fig. 34) can be deduced from the one of stoichiometric perovskite by creation of oxygen vacancies in the SrO-type

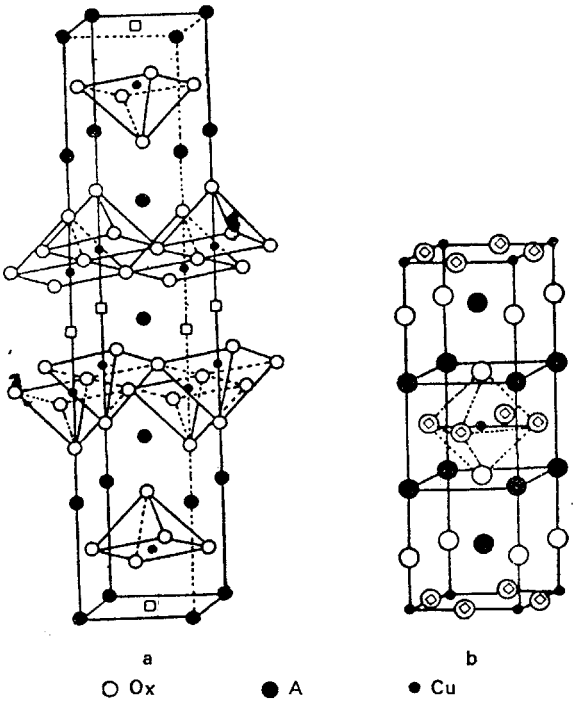

FIG 33 The oxygen deficient intergrowths $AO.[AMO_{3-x}]_n$ (*a*) The oxide $La_2SrCu_2O_6$ ($n = 2$) and (*b*) the oxides $La_{2-x}A_xCu_{1-x/2+\delta}$ (m = 1).

planes in an ordered way. It results that the sequence (AO–CuO_2) along *a* in the cubic perovskite is replaced by the sequence Cu_2O_4–A_2O □–A_2 □$_2$–Cu_2O_4–A_2O □ in $La_3Ba_3Cu_6O_{14}$. In this structure, copper exhibits simulaneously three sorts of coordinations octahedral, pyramidal and square planar. The remarkable feature of this structure concerns the great oxygen defect with respect to perovskite : more than 22 per cent of the anionic sites are unoccupied, in spite of the presence of notable amount of Cu(III). This explains the intercalation properties of this oxides which can intercalate oxygen, without changing its structure. The oxide $La_3Ba_3Cu_6O_{14+\delta}$, like the other mixed valence copper oxides described here, is a *p*-type conductor whose conductivity increases drastically as the amount of intercalated oxygen increases.

The structure of the oxides A_2CuO_3 (Fig. 35*a*) can be generated from the first member of the intergrowth $AO(AMO_3)_n$, i.e. "A_2CuO_4", by elimination of one "plane" of oxygen atoms out of two in the perovskite slab, whereas the SrO-type slabs remain untouched (Fig. 35*b*). This creation of oxygen vacancies leads to the formation of (CuO_2) planes built up from corner-sharing square planar CuO_4 groups. Moreover the (CuO_2) planes are brought closer together, involving a contraction of the AO layers (the *b* parameter perpendicular to the plane of the projection changes from 3.9Å to 3.5Å). It must be pointed out that, no intergrowth between Sr_2CuO_3

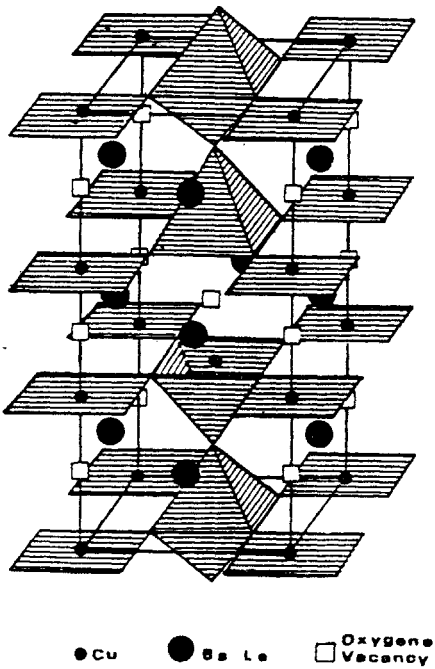

FIG 34 The oxygen deficient perovskite $La_3Ba_3Cu_6O_{14+\delta}$.

and A_2CuO_4 oxides has been observed in spite of the existence of a bidimensional accord along $(010)_{K_2NiF_4}$ between the two structures.

The structural filiation of the oxygen deficient perovskites can be carried on by comparing the structure of $SrCuO_2$ and $SrCu_{0.75}Ni_{0.25}O_2$ (Fig. 36*a*) with that of Sr_2CuO_3 (Fig. 35*a*). This structure consists also of SrO-type slabs and slabs of CuO_4 groups. It exhibits also a bidimensional accord with the Sr_2CuO_3 structure (see Fig. 35a^{100} plane) but it differs from it by the fact that the CuO_4 groups share their edges. The relationship between the two structures can be understood by considering that Sr_2CuO_3 is the first member of the hypothetical series $AO[CuO_2]_n$ obtained by creation of oxygen vacancies in the intergrowth $AO[CuO_3]_n$. The crystallographic shearing of the $(CuO_2)_2$ slab of the second hypothetical member $SrO[CuO_2]_2$ (Fig. 36*b*) leads to the $SrCuO_2$-type structure. Thus, $SrCuO_2$ can be described as a structure derived from the intergrowth of sodium chloride type-ReO_3 type AO ($\square$ MO_3)$_2$ by an ordered creation of rows of oxygen atoms in the ReO_3-type slab followed by a crystallographic shear operation in this slab.

The oxide $CaCu_2O_3$ (Fig. 37) exhibits also a similiarity with Sr_2CuO_3 and $SrCuO_2$ as shown by the presence of layers of CuO_4 groups. However, it differs from the other two structures by the absence of SrO-type slabs. One observes Cu_2O_3 planes built up from distorted square planar groups CuO_4, sharing sometimes their corners like in Sr_2CuO_3, and sometimes their edges like in $SrCuO_2$. In fact

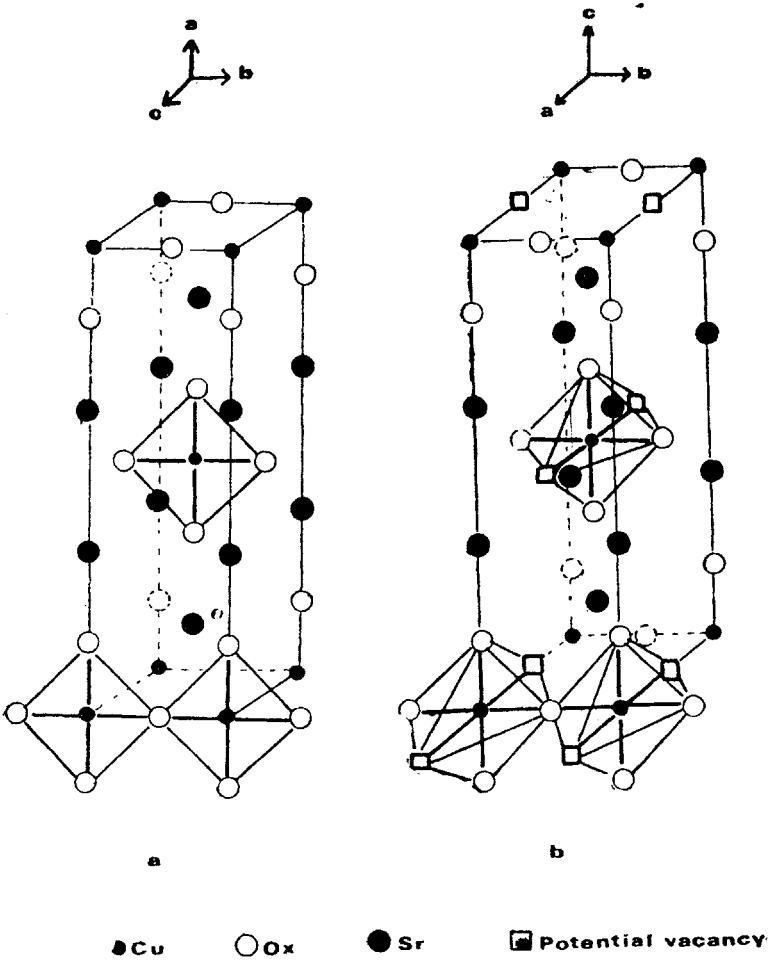

FIG. 35 The structure of Sr_2CuO_3 (*a*) can be deduced from the K_2NiF_4-type structure (*b*) by elimination of one "plane" of oxygen atoms out of two (□) parallel to $(010)_{K_2NiF_4}$.

this structure is closely related to the W_nO_{3n-1} shear structures characterized by one sort of {001} CSP. Its layers Cu_2O_3 can be deduced from the hypothetical member $m = 2$ ("W_2O_5") (Fig. 38*a*) by suppression of the oxygen atoms located on both sides of the CuO_4 basal plane of the octahedra (Fig. 38*b*), and then by bringing the Cu_2O_3 layers closer together. The calcium ions are inserted in the octahedral cavities formed by the CuO_4 groups.

Other Oxygen-Defect Perovskites[3,133–135]

Other oxygen-defect perovskites have been isolated, whose structure is not completely determined to our knowledge : besides oxides such as $SrTiO_{2.5}$ and $SrVO_{2.5}$, the oxides $La_nNi_nO_{3n-1}$ seem to be very promising.

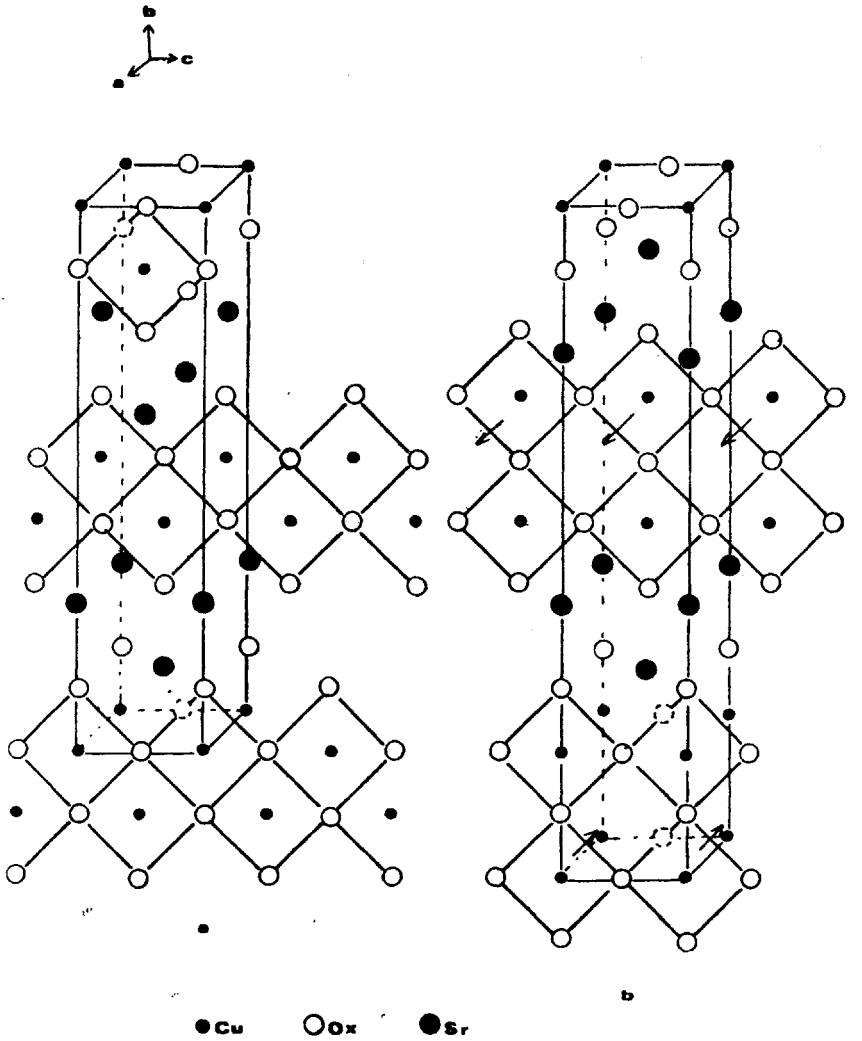

FIG 36 The structure of $SrCuO_2$ (*a*) and the hypothetical structure of the member $n = 2$ of the hypothetical series $AO(CuO_2)_n$. (*b*) The arrows correspond to the direction of the shearing.

CONCLUSION

The ReO_3-type structure can be considered as a very important precursor in the generation of new structural families. New structures can indeed be generated from this very simple and flexible framework in different manners : deformation of the framework by compression without major distortion of the octahedra, shearing phenomena, ordered formation of anionic vacancies, intergrowth resulting from a bidimensional accord with other structures, adaptability to other polyhedra and especially to tetrahedra. From this structural affiliation it appears that the ReO_3-

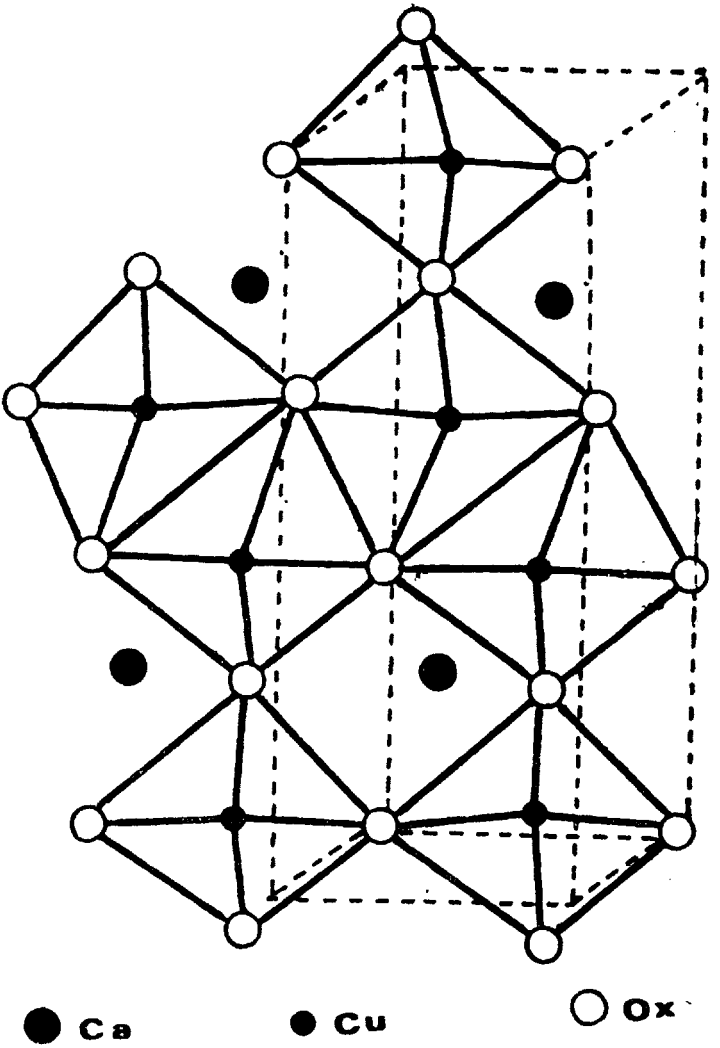

FIG 37 The structure of $CaCu_2O_3$.

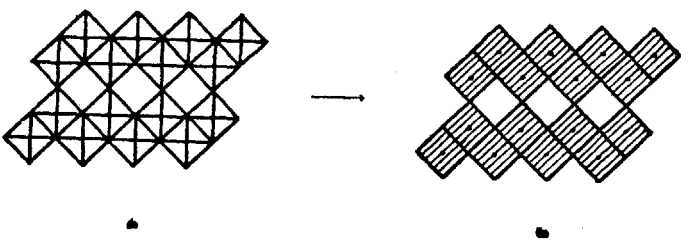

FIG 38 The transformation of the "W_2O_5" shear structure (*a*) into the "Cu_2O_3" layers (*b*) by ordered elimination of oxygen atoms.

type framework is closely related to the structure of different oxides such as the MO oxides with rock-salt structure, anatase and β-cristoballite.

It is also clear that the octahedral "M_4O_{20}" limits can be considered as fundamental structural units which can participate to the edification of numerous structures of oxides. Perovskite columns built up from such "M_4O_{20}" units can indeed be recognized in many oxides which have not been described here, such as molybdenum and tungsten oxides with a tunnel structure, V_6O_{13}, Na_xTiO_3 bronzes, $BaTi_2O_5$ and so on.

It must finally be emphasized that another aspect of this structure has not been analyzed here : its relationship with the close-packed oxides. The consideration of the ReO_3-type structure along the {111} direction of the cubic cell and the insertion in the lattice of a A cation with the same size as that of oxygen (A = Ba^{2+}, K^+) leads to a description of the structure in terms of an ABC close-packing of AO_3 layers, which form octahedral sites where the M ions of the AMO_3 perovskite are located. Many cation deficient "perovskites" $AM_{1-x}O_3$ correspond to this description : they are characterized by a regular stacking of AO_3 layers and the M cations and vacancies exhibit generally an ordered distribution in the octahedral sites, involving often the presence of face-sharing octahedra, and a hexagonal symmetry of superstructures. In the same way several hexagonal perovskites such as $BaMO_{3-x}$ (M = Mn, Fe, Co) exhibit oxygen defects with for some of them an ordered distribution. All these "close-packed perovskites" are closely related to the different close-packings observed for other oxides. The study of the relationships between these different close-packed structures covers a wide field which cannot be developed here. Many oxides derived from the ReO_3-type structure exhibit interesting electron transport, magnetic, or catalytic properties. Thus, it appears that the systematic investigation of different systems of oxides, in a predictive manner, should allow to isolate new materials with specific properties and to establish a correlation between the structure and their properties.

References

1. F Galasso *Structure, Properties and Preparation of Perovskite-type Compounds* Pergamon Press (1969)
2. A F Wells *Structural Inorganic Chemistry* Clarendon Press Oxford (1975)
3. C N R Rao J Gopalakrishnan and K Vidyasagar *Indian J Chem* **23A** (1984) 265
4. P Hagenmuller *Progr Solid State Chem* **5** Pergamon Press (1971) p. 71–144
5. A D Wadsley *Non-stoichiometric Compounds* (Ed L Mandelcorn) Academic Press (1964) p. 98 to 209
6. T Ekström and R J D Tilley *Chemica Scripta* **16** (1980) 1
7. M Marezio P D Dernier J Chenavas and J C Joubert *J Solid State Chem* **6** (1973) 16
8. B Bochu J Chenavas J C Joubert and M Marezio *J Solid State Chem* **11** (1974) 88
9. J Chenavas J C Joubert M Marezio and B Bochu *J Solid State Chem* **14** (1975) 25
10. A Deschanvres B Raveau and F Tollemer *Bull Soc Chim Fr* **11** (1967) 4077
11. B Bochu M N Deschizeaux J C Joubert A Collomb J Chenavas and M Marezio *J Solid State Chem* **29** (1979) 291

12. C N R Rao D J Buttrey N Otsuka P Ganguly H R Harrison C J Sandberg and J M Honig *J Solid State Chem* **51** (1984) 266
13. B Grande H K Müller-Buschbaum and M Schweitzer *Z anorg allg Chem* **428** (1977) 120
14. R J D Tilley *J Solid State Chem* **21** (1977) 293
15. R Collongues *La non-stoechiométrie* (*Ed* Masson) Paris (1971)
16. S R Ruddlesden and P Popper *Acta Cryst* **10** (1957) 538 and **11** (1958) 54
17. J J Randall L Katz and R Ward *J Am chem Soc* **79** (1957) 266
18. A Rabenau and P Eckerlin *Acta Cryst* **11** (1958) 304
19. G Wagner and M Binder *Z anorg allg Chem* **298** (1959) 12
20. R Weiss and R Faivre *CRAS* **248** (1959) 106
21. A Magnéli *Acta Chem Scand* 7 (1953) 315
22. A Hussain and L Kihlborg *Acta Cryst* **A32** (1976) 551
23. L Kihlborg *Chem Scripta* 14 (1979) 187
24. R Sharma and L Khilborg *Mat Res Bull* **16** (1981) 377
25. R Steadman R J D Tilley and I J Mc Colm *J Solid State Chem* **4** (1972) 199
26. T Ekstrom M Parmentier and R J D Tilley *J Solid State Chem* **37** (1981) 24; and **24** (1978) 209; and **28** (1979) 259
27. L Kihlborg and R Sharma *J Microsp Spectroscop Electron* 7 (1982) 387
28. M Parmentier C Gleitzer and R J D Tilley *J Solid State Chem* **31** (1980) 305
29. M Ganne M Dion A Verbaere and M Tournoux *J Solid State Chem* **29** (1979) 9
30. A Benmoussa D Groult F Studer and B Raveau *J Solid State Chem* **41** (1982) 221
31. B Raveau *Rev inorg Chem* **1** (1979) 81
32. L Kihlborg M Sundberg and A Hussain *Chem Scripta* **15** (1980) 182
33. A Magnéli *Arkiv Kemi* **1** (1949) 213
34. B G Hyde and M O'Keeffe *Acta Cryst* **A29** (1973) 243
35. B G Hyde A V Bagshaw S Andersson and M O'keeffe *Ann Rev Mater Sci* **4** (1974) 43
36. A Sleight and A Magnéli *Acta Chem Scand* **18** (1964) 2007
37. D C Craig and N C Stephenson *Acta Cryst* **B25** (1969) 2071
38. S Iijima and I G Allpress *Acta Cryst* **A30** (1974) 22 and 30
39. H Obayashi and J S Anderson *J Solid State Chem* **17** (1976) 79
40. S Iijima *Acta Cryst* **A34** (1978) 922
41. S Horiuchi K Muramatsu and Y Matsui *Acta Cryst* **A34** (1978) 939
42. T Ekström and R J D Tilley *J Solid State Chem* **18** (1976) 123
43. A Sleight *Acta Chem Scand* **20** (1966) 1102
44. A D Wadsley and S Andersson *Perspectives in Structural Chemistry* **3** (*Ed* J D Dunitz and J A Ibers) John Wiley & Sons (1970) p 1 to 58
45. A Magneli *Acta Cryst* **6** (1953) 495
46. J S Anderson In : *Surface and Defect Properties of Solids* (*Ed* M W Roberts and J M Thomas) Vol. **1** The Chemical Society London (1972)
47. R J D Tilley In : *MTP int Rev Sci Inorg Chem Ser* 1 **10** (*Ed* L E J Roberts) Butterworths London (1972)
48. J S Anderson and R J D Tilley In : *Surface and Defect Properties of Solids* (*Ed* M W Roberts and J M Thomas) Vol. **3** The Chemical Society London (1974)
49. R J D Tilley In : *MTP Int Rev Sci inorg Chem Ser* 2 **10** (*Ed* L E J Roberts) Butterworths London (1974)
50. T Ekstrom and R J D Tilley *Mater Res Bull* **9** (1974) 705
51. R J D Tilley *Mat Res Bull* **5** (1970) 813
52. B Blomberg L Kihlborg and A Magneli *Arkiv Kemi* **6** (1953) 133
53. S Iijima *J Solid State Chem* **14** (1975) 52
54. J G Allpress R J D Tilley and M J Sienko *J Solid State Chem* **3** (1971) 440

55. J D Allpress *J Solid State Chem* **4** (1972) 173
56. M Sundberg *Acta Cryst* **B32** (1976) 2144 and *J Solid State Chem* **35** (1980) 120
57. M Sundberg and R J D Tilley *J Solid State Chem* **11** (1974) 150
58. P J England J Booth R J D Tilley and T Ekström *J Solid State Chem* **44** (1982) 60
59. W Sahle and M Sundberg *Chem Scripta* **22** (1983) 248
60. L A Bursill *J Solid State Chem* **6** (1973) 195
61. L A Bursill *J Solid State Chem* **48** (1983) 256
62. J G Allpress J V Sanders and A D Wadsly *Acta Cryst* **B25** (1969) 1156
63. M Nanot F Queyroux J C Gilles and R Chevallier *Acta Cryst* **B32** (1976) 115
64. R Portier A Carpy M Fayard and J Galy *Phys Status Sol* **A30** (1975) 683
65. M Nanot F Queyroux J C Gilles R Portier and M Fayard *Mater Res Bull* **10** (1975) 313
66. J K Brandon and H D Megaw *Phil Mag* **21** (1970) 189
67. M Nanot F Queyroux J C Gilles A Carpy and J Galy *J Solid State Chem* **11** (1974) 272
68. B Aurivillius *Arkiv Kemi* **1** (1949) 463
69. E C Subbarao *J Phys Chem Soc* **23** (1962) 665
70. R E Newnham R W Wolfe and J F Dorrian *Mater Res Bull* **6** (1971) 1029
71. I G Ismailzade V I Nesterenko F A Mirishli and P G Rustamov *Sov Phys Crystallogr* **12** (1967) 400
72. S Horiuchi K Muramatsu and M Shimazu *J Solid State Chem* **34** (1980) 51
73. J L Hutchison J S Anderson and C N R Rao *Proc R Soc London* **A355** (1977) 301
74. M M Hey F A Bannister and J Russel *Min Mag* **25** (1938) 41
75. E L Galperin L Y Erman I K Kolchin M A Belova and K S Chernyshev *Russ J inorg Chem* **11** (1966) 1137
76. Y Bando A Watanabe Y Sekikawa M Goto and S Horiuchi *Acta Cryst* **A35** (1979) 142
77. D A Jefferson J Gopalakrishnan and A Ramanan *Mater Res Bull* **17** (1982) 269
78. L Kihlborg *Arkiv Kemi* **21** (1963) 357
79. J P Giroult M Goreaud Ph Labbe and B Raveau *Acta Cryst* **B37** (1981) 2139 and 1163
80. J P Giroult M Goreaud Ph Labbe J Provost and B Raveau *Mat Res Bull* **16** (1981) 811
81. J P Giroult M Goreaud Ph Labbe and B Raveau *Acta Cryst* **B38** (1982) 2342
82. M Hervieu and B Reveau *J Solid State Chem* **43** (1982) 299
83. J P Giroult M Goreaud Ph Labbe and B Raveau *J Solid State Chem* **44** (1982) 407 and *Rev Chim Miner* **20** (1983) 829
84. Ph Labbe D Ouaehee M Goreaud and B Raveau *J Solid State Chem* **50** (1983) 163
85. B Domenges M Goreaud Ph Labbe and B Raveau *J Solid State Chem* **50** (1983) 173
86. M Hervieu and B Raveau *Chem Scripta* **22** (1983) 117 and 123
87. A Benmoussa D Groult Ph Labbe and B Reveau *Acta Cryst* **C40** (1984) 573
88. B Domenges M Hervieu and B Raveau *Acta Cryst* **B40** (1984) 249
89. B Domenges M Hervieu R J D Tilley and B Raveau *J Solid State Chem* **54** (1984) 10
90. M Hervieu B Domenges R J D Tilley and B Raveau *J Solid State Chem* **57** (1985)
91. B Domenges M Goreaud Ph Labbe and B Raveau *Acta Cryst* **B38** (1982) 1724
92. M Goreaud Ph Labbe and B Raveau *J Solid State Chem* **56** (1985) 41
93. L Kihlborg *Arkiv Kemi* **21** (1963) 365
94. A Magneli *Acta Chem Scand* **2** (1948) 861
95. D Groult M Hervieu and B Raveau *To be published*
96. B M Gatehouse *J Less Common Metals* **36** (1974) 53
97. N C Stephenson *Acta Cryst* **20** (1966) 59
98. B M Gatehouse and D J Lloyd *J chem Soc chem Comm* **13** (1971)
99. E F Bertaut P Blum and A Sagnieres *Acta Cryst* **12** (1959) 149
100. J Bergren *Acta Chem Scand* **25** (1971) 3616

101. J C Grenier G Schiffmacher P Caro M Pouchard and P Hagenmuller *J Solid State Chem* **20** (1977) 365
102. J C Grenier M Pouchard and P Hagenmuller *Structure and Bonding* **47** (1981) 1
103. K Vidyasagar J Gopalakrishnan and C N R Rao *Inorg Chem* **23** (1984) 1206
104. J C Grenier S Ghodbane G Demazeau M Pouchard and P Hagenmuller *Mater Res Bull* **14** (1979) 831
105. J B MacChesney R C Sherwood and J F Potter *J chem Phys* **43** (1965) 1907
106. B C Tofield C Greaves and B E Fender *Mater Res Bull* **10** (1975) 737
107. M A Alario-Franco J C Joubert and J P Levy *Mater Res Bull* **17** (1982) 733
108. J C Grenier J Darriet M Pouchard and P Hagenmuller *Mater Res Bull* **11** (1976) 1219
109. Y Bando Y Sekikawa H Nakamara and Y Matsui *Acta Cryst* **A37** (1981) 723
110. M A Alario-Franco M J R Henche M V Regi J M G Calbet J C Grenier A Wattiaux and P Hagenmuller *J Solid State Chem* **46** (1983) 23
111. M A Alario-Franco I M G Calbet M V Regi and J C Grenier *J Solid State Chem* **49** (1983) 219
112. J M G Calbet M V Regi M A Alario-Franco and J C Grenier *Mater Res Bull* **18** (1983) 285
113. N Nguyen Y Calage F Varret G Ferey V Caignaert M Hervieu and B Raveau *J Solid State Chem* **53** (1984) 398
114. M Hervieu N Nguyen V Caignaert and B Raveau *Phys Stat Sol* **A83** (1984) 473
115. K R Poeppelmeier M E Leonowicz and J M Longo *J Solid State Chem* **44** (1982) 89
116. K R Poeppelmeier M E Leonowicz J C Scanlon J M Longo and W B Yelon *J Solid State Chem* **45** (1982) 71
117. A Reller D A Jefferson J M Thomas and M K Uppal *Proc R Soc London* **A394** (1984) 224
118. A Reller D A Jefferson J M Thomas and M K Uppal *J phys Chem* **87** (1983) 913
119. V Caignaert N Nguyen M Hervieu and B Raveau *Mater Res Bull* **20** (1985) 479 and *J Solid State Chem* (1985)
120. N Nguyen L Er Rakho C Michel J Choisnet and B Raveau *Mater Res Bull* **15** (1980) 891
121. N Nguyen J Choisnet M Hervieu and B Raveau *J Solid State Chem* **39** (1981) 120
122. N Nguyen J Choisnet and B Raveau *Mater Res Bull* **17** (1982) 567
123. N Nguyen C Michel F Studer and B Raveau *Mater Chem* **7** (1982) 413
124. N Nguyen F Studer and B Raveau *J Phys Chem Solids* **44** (1983) 389
125. C Michel L Er-Rakho and B Raveau *Mater Res Bull* (1985)
126. L Er-Rakho C Michel J Provost and B Raveau *J Solid State Chem* **37** (1981) 151
127. J Provost F Studer C Michel and B Raveau *Synthetic Metals* **4** (1981) 147 and 157
128. C Michel and B Raveau *Rev Chim Miner* **21** (1984) 407
129. L Teske and H K Muller-Buschbaum *Z anorg allg Chem* **371** (1969) 325
130. L Teske and H K Muller-Buschbaum *Z anorg allg Chem* **379** (1970) 234
131. H K Müller-Buschbaum and H J Mattausco *Z anorg allg Chem* **377** (1970) 144
132. L Teske and H K Müller-Buschbaum *Z anorg allg Chem* **370** (1969) 135
133. P L Gai and C N R Rao *Naturforsch* **30A** (1975) 1092
134. M A Alario-Franco and M V Regi *Nature* **270** (1977) 706
135. B C Tofield *Nature* **272** (1978) 713